time-dependent manner, with a $T_{1/2}$ of 15 min (Figure 4B). These data suggest that forskolin promotes FCoR nuclear localization in HEK293 cells. Furthermore, we investigated subcellular localization of endogenous FCoR in 3T3-F442A cells during differentiation. At 48 h after induction, in the presence of 3-isobutyl-1-methylxanthine (IBMX), which is a competitive non-selective phosphodiesterase inhibitor and raises intracellular cAMP and activates PKA, FCoR was localized in nucleus and, thereafter, moved to cytosol (Figure 4C). These data support the observation that PKA induces nuclear accumulation of FCoR.

We next examined whether forskolin induced FCoR phosphorylation. Sequence analysis revealed a consensus protein kinase A (PKA) phosphorylation site (R/K-X_{1-2}-**S/T**-X) at

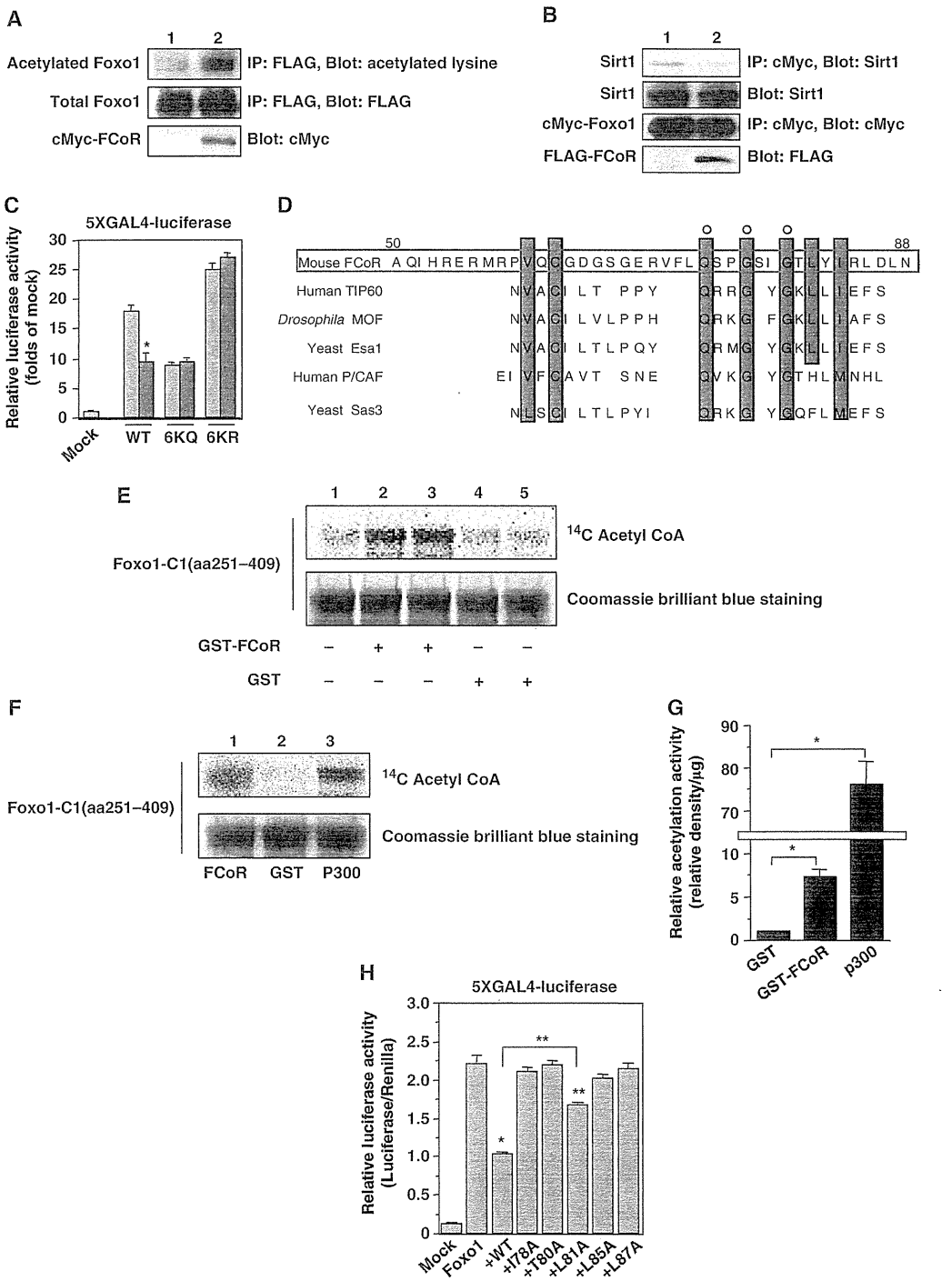

Threonine 93 (Supplementary Figure S1B). Forskolin rapidly induced FCoR phosphorylation (Figure 4D) in a H-89-inhibitable manner (H89 inhibits PKA) (Figure 4E; Lochner and Moolman, 2006).

Site-directed mutagenesis of Serine 92 or/and Threonine 93 to Alanine (S92A, T93A, or S92A/T93A) indicated that Threonine 93, but not Serine 92, is phosphorylated in response to forskolin (Figure 4F). To confirm that Threonine 93 is phosphorylated by forskolin, we generated a site-specific phospho-T93 antibody (pT93). pT93 immunoreactivity increased in response to forskolin (Figure 4G), suggesting that the main site of FCoR that is phosphorylated in response to forskolin is Threonine 93. Furthermore, the PKA catalytic subunit phosphorylated the GST-WT FCoR fusion protein directly, but did not phosphorylate GST-T93A or -T93D FCoR fusion protein (Figure 4H). These data suggest that PKA directly phosphorylates Threonine 93.

FCoR has a predicted nuclear export signal (NES; amino acids 78–87) (Supplementary Figure S4A). Indeed, substitution of Leucine 81 with Alanine enhances FCoR nuclear translocation and inhibits Foxo1 activity in the absence of forskolin (Supplementary Figure S4B and C). This indicates that Leucine 81 is important for NES. We hypothesized that Threonine 93 phosphorylation affects the subcellular localization of FCoR. Immunofluorescence of cells transfected with the T93A and T93D FCoR mutants revealed that T93A FCoR localized mainly to the cytosol, while T93D FCoR was mainly in the nucleus (Figure 4I). Furthermore, Western blotting of cytosolic and nuclear extracts of HEK293 cells transfected with WT-, T93A-, or T93D-FCoR in the absence of forskolin supported these findings (Figure 4J). We performed 5XGAL4 luciferase assays using WT-, T93A-, or T93D-FCoR. FoxO1 increased 5XGAL4 luciferase activity by 17-fold, while co-transfection with WT FCoR decreased transcriptional activity by 40%. The T93D-FCoR mutant decreased transcriptional activity more markedly than WT or T93A-FCoR (Figure 4K). Inhibition of Foxo1 activity by FCoR reflects the Foxo1 acetylation level. An *in-vivo* acetylation assay in HEK293T cells demonstrated that T93D FCoR acetylated Foxo1 the most (Figure 4L). Taken together, these data indicate that phosphorylation of Threonine 93 induces FCoR nuclear localization and leads to the acetylation and inhibition of Foxo1.

Finally, to investigate regulation of the interaction between Foxo1 and FCoR, we performed co-immunoprecipitation studies with or without forskolin in the presence of serum. In the presence of forskolin, FCoR did not bind to Foxo1 (Figure 4M, left panel). In contrast, in the absence of forskolin, FCoR bound to Foxo1 (Figure 4M, right panel). Furthermore, in the absence of serum and the presence of forskolin, FCoR bound to Foxo1 (Figure 2E). These data indicate that the interaction between FCoR and Foxo1 depends on their subcellular localization.

FCoR is required for adipocyte differentiation

To investigate the physiological role of FCoR in adipocyte differentiation, we inhibited endogenous FCoR in 3T3-F442A cells using adenoviruses encoding two kinds of small hairpin (sh)RNA to decrease FCoR expression (Figure 5B and C; Supplementary Figure S5B and C). Oil-red O staining revealed that knockdown of endogenous FCoR inhibited the differentiation of 3T3-F442A cells (Figure 5A; Supplementary Figure S5A). Analysis of the expression of adipocyte-specific genes demonstrated reduced levels of *Pparγ* (*Pparg*), *Glut4* (*Slc2a4*), and *adiponectin* (*Adipoq*) (Figure 5D; Supplementary Figure S5D). We showed previously that CN Foxo1 inhibits adipocyte differentiation (Nakae *et al*, 2003). If FCoR inhibits Foxo-dependent transcription, then knockdown of FCoR should enhance the expression of Foxo1-target genes. Indeed, real-time PCR analysis demonstrated that expression levels of several Foxo1-target genes increased in cells transduced with FCoR shRNA compared with scrambled shRNA-transduced cells (Figure 5E; Supplementary Figure S5E). To examine whether FCoR interacts with Foxo1 *in vivo*, we performed chromatin immunoprecipitation (Chip) assay using the *p21* (*Cdkn1a*) promoter (Nakae *et al*, 2003). The Chip assay demonstrated that FCoR interacted with *Cdkn1a*

Figure 3 FCoR enhances Foxo1 acetylation. (**A**) Effect of FCoR on Foxo1 acetylation. After transfection with pFLAG-CMV2-WT Foxo1 with or without pCMV5-cMyc-WT FCoR, HEK293 cells were incubated with H_2O_2 (500 μM), nicotinamide (NAM) (50 mM), and trichostatin A (TSA) (2 μM) for 3 h and harvested. Lysates were immunoprecipitated with anti-FLAG mouse monoclonal antibody (M2) and subjected to western blotting with the indicated antibodies. The bottom panel shows western blotting of the lysates with and anti-cMyc mouse monoclonal antibody. (**B**) FCoR disrupts the interaction between Foxo1 and Sirt1. After transfection with pCMV5-cMyc-WT Foxo1 and pTOPO-Sirt1 with or without pCMV5-cMyc-WT FCoR, HEK293 cells were incubated with H_2O_2 for 3 h and harvested. Cell lysates were immunoprecipitated with an anti-cMyc mouse monoclonal antibody and subjected to western blotting with the indicated antibodies. (**C**) 5XGAL4-luciferase assay of PM-WT, -6KQ, and -6KR Foxo1. At 36 h after transfection with pTAL-5XGAL4, phRL-SV40, and the indicated PM-Foxo1 with or without the FCoR expression vector, HEK293 cells were incubated with forskolin (20 μM) for 6 h and harvested. Luciferase activity was measured in the cell lysates. The grey bar indicates mock-transfected cells and the blue bar indicates pCMV5-cMyc-WT FCoR-transfected cells. Data represent the mean values ± s.e.m. from three independent experiments. Asterisk indicates statistically significant difference (*$P<0.005$ by one-way ANOVA). (**D**) Sequence alignment of FCoR with various acetyltransferases. Residues that are identical or chemically similar to those in mouse FCoR are shown with a red background. FCoR has sequence similarity to the acetyl-CoA binding motifs of the MYST family of HATs (yeast Esa1, yeast Sas3, *Drosophila* MOF, human TIP60, and human P/CAF). (**E**) *In-vitro* acetylation assay of Foxo1. The GST-Foxo1-C1 (aa251–409) protein was subjected to *in-vitro* acetylation assays with GST (lanes 1, 4, and 5) or GST-FCoR (lanes 2 and 3) as described in 'Materials and methods'. Reaction products were analysed by Coomassie brilliant blue staining and autoradiography (^{14}C). (**F**) *In-vitro* acetylation assay of Foxo1. The GST-Foxo1-C1 (aa251–409) protein was subjected to *in-vitro* acetylation assays with GST-FCoR (lane 1), GST (lane 2), or recombinant p300 (lane 3) as described in 'Materials and methods'. Reaction products were analysed by Coomassie brilliant blue staining and autoradiography (^{14}C). (**G**) Quantification of acetylation activity of FCoR. The intensity of each acetylated band and Coomassie brilliant blue staining band was measured by NIH Image1.62. The relative intensity was corrected by the weight of GST-FCoR or recombinant p300. Data represent the mean values ± s.e.m. from two independent experiments. An asterisk indicates statistically significant differences (*$P<0.001$ by one-way ANOVA). (**H**) 5XGAL4-luciferase assay of PM-Foxo1 with pCMV5/cMyc-WT, I78A, T80A, L81A, L85A, and L87A FCoR. At 36 h after transfection with pTAL-5XGAL4, phRL-SV40, and the indicated PM-Foxo1 with or without the FCoR expression vector, HEK293 cells were incubated with forskolin (20 μM) for 6 h and harvested. Luciferase activity was measured in the cell lysates. Data represent the mean values ± s.e.m. from three independent experiments. Asterisks indicate statistically significant differences (*$P<0.001$ and **$P<0.05$ by one-way ANOVA). Figure source data can be found with the Supplementary data.

in a differentiation time-dependent manner (Figure 5F). Furthermore, adenoviruses encoding FCoR significantly enhanced acetylation of endogenous Foxo1 at day 4 after induction of differentiation in 3T3-F442A cells (Figure 5G) and significantly increased *Pparg* expression at day 10 (Figure 5A; Supplementary Figure S6A).

Foxo1 inhibits the ligand-dependent transcriptional activation of PPARγ. Therefore, if FCoR inhibits Foxo1 activity, then

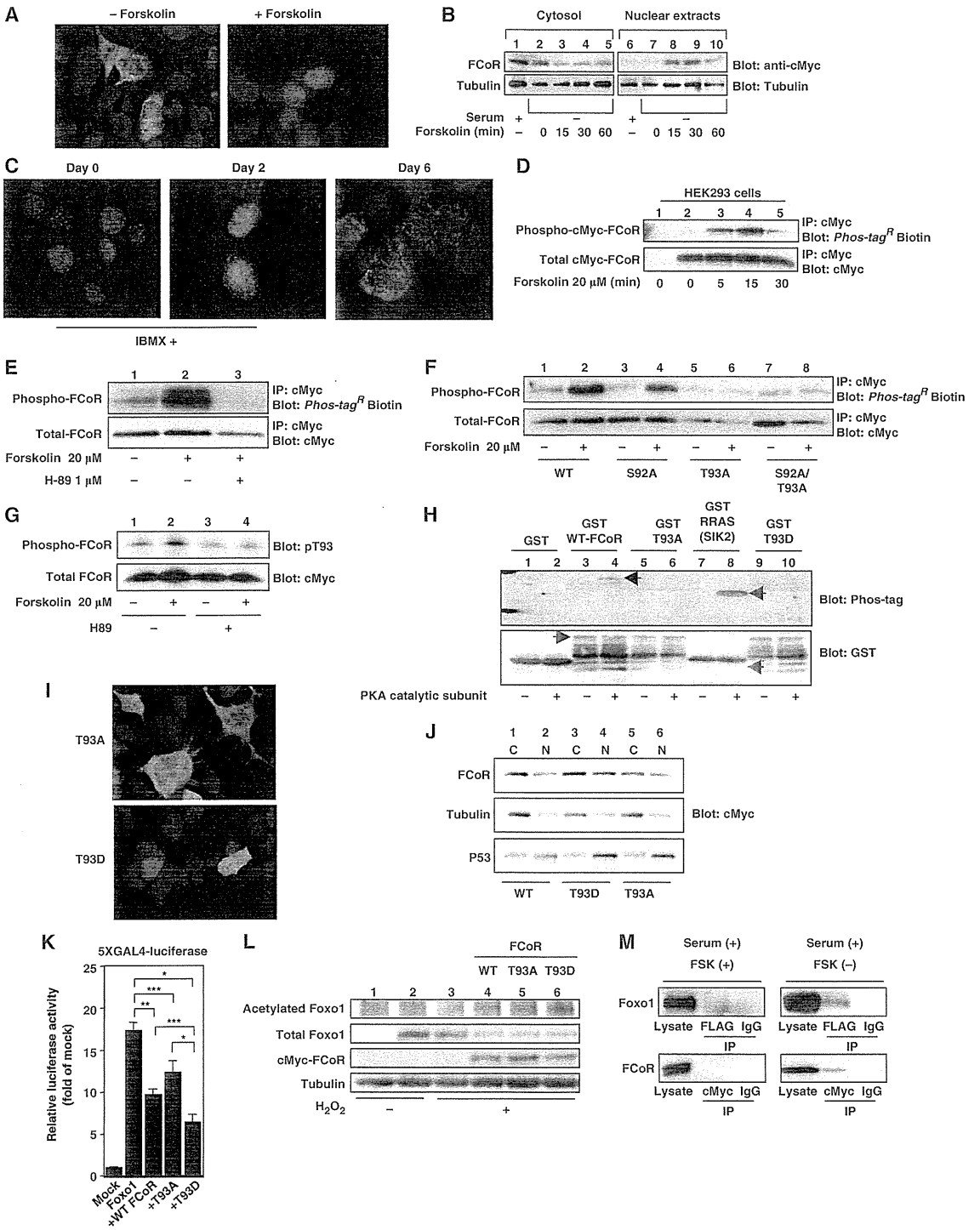

FCoR should prevent Foxo1-mediated inhibition of PPARγ. A Luciferase assay using the J3-tk-Luc reporter vector, which contains three copies of the PPAR response element (PPRE) of the apolipoprotein A-II gene J site, demonstrated that FCoR did not prevent inhibition of PPARγ by Foxo1 (Supplementary Figure S6B). These data suggest that FCoR affects adipocyte differentiation, but not through the interaction of Foxo1 and PPARγ.

Overexpression of FCoR in WAT decreased adiposity and increased insulin sensitivity

To study the function of FCoR *in vivo*, we generated transgenic mice that overexpressed FCoR in their adipose tissue (*aP_2-cMyc-Fcor*: RIKEN Acc. No. CDB0446T) using the 5.4-kb promoter-enhancer fragment of the mouse *aP_2* (Figure 6A; Abel *et al*, 2001; Imai *et al*, 2001; He *et al*, 2003). We characterized two founder lines; line 1 (*WFCoR*) showed greater expression in WAT than in BAT, while the reverse was true for line N5 (*BFCoR*) (Figure 6B–D). We thus used *WFCoR* to study the role of FCoR in WAT and *BFCoR* to study the role of FCoR in BAT.

WFCoR mice showed an adult-onset decrease in weight loss (Figure 6E). CT scan revealed that *WFCoR* mice had decreased adipose mass, including the visceral and subcutaneous depots (Figure 6F). Histological analysis of WAT from these animals demonstrated that the adipocytes in the WAT of *WFCoR* mice were similar to WT mice at 12 weeks but the adipocytes in the WAT of *WFCoR* mice were smaller than those from WT mice at 24 weeks (Figure 6G; Supplementary Figure S7A and B). Although food intake, locomotor activity, and oxygen consumption were similar to wild-type mice, the respiratory quotient of *WFCoR* mice was significantly reduced (Figure 6H, and data not shown). These data indicate increased usage of lipid as an energy source, resulting in lower body weight.

To investigate the effects of FCoR overexpression in WAT on glucose metabolism, we performed intraperitoneal glucose (IPGTT) and insulin tolerance test (ITT). Two-month-old *WFCoR* mice showed the same glucose tolerance and insulin sensitivity as wild-type mice (data not shown). However, 4-month-old mice showed evidence of increased glucose (Figure 6I) and insulin tolerance (Figure 6J). Insulin secretion in *WFCoR* mice was similar to that of wild-type mice during IPGTT (Supplementary Figure S8). These data suggest that overexpression of FCoR in WAT decreases adiposity and increases insulin sensitivity in an age-dependent manner.

To investigate the mechanism by which FCoR increases insulin sensitivity, we examined the expression levels of adipose tissue-specific and Foxo1-target genes in WAT. FCoR transgenic mice showed increased *Pparg* and decreased *Tnf-α* (*Tnf*), *Mcp-1* (*Ccl2*), and *Ccr2* gene expression (Figure 6J and K). Expression of several Foxo1-target genes (Greer and Brunet, 2005) was decreased, including the expression of *p27* (*Cdkn1b*), *Rb1*, *p130* (*Rbl2*), *Cyclin G2* (*Ccng2*), *fas ligand* (*fasl*), *Bcl2l11*, *Gadd45* (*Gadd45a*), *Sod2*, and *Cat* was decreased (Figure 6L). Acetylation of endogenous Foxo1 in WAT was significantly increased compared with wild-type mice (Figure 6M). These data suggest that overexpression

Figure 4 FCoR is phosphorylated and translocated into the nucleus in a PKA-dependent manner. (**A**) Subcellular localization of exogenous FCoR in HEK293 cells. At 36 h after transfection with pCMV5-cMyc-WT FCoR, HEK293 cells were stimulated with forskolin (20 μM) for 30 min, fixed, and stained with anti-cMyc mouse monoclonal antibody. (**B**) Western blotting of cytosolic and nuclear extracts from HEK293 cells transfected with cMyc-FCoR. At 36 h after transfection with pCMV5-cMyc-WT FCoR, HEK293 cells were stimulated with forskolin (20 μM) at the indicated time and harvested. Lysates were fractionated into cytosolic and nuclear extracts and subjected to western blotting with the indicated antibodies. (**C**) Immunofluorescence of endogenous FCoR in 3T3-F442A cells. 3T3-F442A cells were cultured and induced differentiation into mature adipocytes as described in Materials and Methods except supplementation with 500 nM of IBMX for 48 h. Thereafter, cells were cultured in DMEM containing 10% fetal calf serum and 1.7 μM of insulin. Cells were fixed at the indicated days and stained with anti-FCoR rabbit polyclonal antibody. (**D**) Phosphorylation of FCoR by forskolin. After transfection with pCMV5-cMyc-WT FCoR, HEK293 cells were stimulated with forskolin (20 μM) at the indicated time and harvested. Cell lysates were immunoprecipitated with anti-cMyc mouse monoclonal antibody, subjected to western blotting, and phosphorylated FCoR was detected. (**E**) Inhibition of phosphorylation of FCoR by H89. At 48 h after transient transfection with pCMV5-cMyc-WT FCoR, HEK293 cells were incubated with or without H89 (1 μM) for 3 h and stimulated with forskolin (20 μM) for 15 min and harvested. Phosphorylated FCoR was detected as described above. (**F**) Phosphorylation of mutant FCoR. After transfection with pCMV5-cMyc-WT (lanes 1 and 2), S92A (lanes 3 and 4), T93A (lanes 5 and 6), or S92A/T93A (lanes 7 and 8) FCoR, HEK293 cells were stimulated with forskolin (20 μM) for 15 min. Phosphorylated FCoR was detected as described above. (**G**) Detection of phosphorylated Threonine 93 by anti-phospho-T93-specific (anti-pT93) antibody. At 48 h after transfection with pCMV5-cMyc-WT FCoR, HEK293 cells were incubated with or without H89 (1 μM) for 3 h and stimulated with or without forskolin (20 μM) for 15 min and harvested. Lysates were subjected to western blotting with anti-pT93. (**H**) *In-vitro* phosphorylation assay of FCoR. GST, GST-WT, GST-T93A, GST-T93D FCoR, and GST-RRAS, which is a short sequence of salt-inducible kinase (SIK) 2, was phosphorylated *in vitro* by incubating with a catalytic subunit from cAMP-dependent protein kinase as described in 'Materials and methods'. Reaction products were subjected to western blotting, phosphorylated products were detected using *Phos-tag*^{R} BTL-104 (top panel) and then blotted with anti-GST antibody (bottom panel). (**I**) Subcellular localization of exogenous T93A (the top panel) or T93D FCoR (the bottom panel) in HEK293 cells. At 36 h after transfection with pCMV5-cMyc-T93A or T93D FCoR, HEK293 cells were fixed as described in Materials and methods and stained with anti-cMyc mouse monoclonal antibody. (**J**) Western blotting of cytosolic and nuclear extracts from HEK293 cells transfected with cMyc-WT (lanes 1 and 2), T93D (lanes 3 and 4), or T93A (lanes 5 and 6) FCoR. At 36 h after transfection, HEK293 cells were harvested. Lysates were fractionated into cytosolic and nuclear extracts and subjected to western blotting with the indicated antibodies. (**K**) 5XGAL4-luciferase assay of PM-Foxo1 with pCMV5/cMyc-WT, T93A, and T93D FCoR. At 36 h after transfection with pTAL-5XGAL4, phRL-SV40, and the indicated PM-Foxo1 with or without the FCoR expression vector, HEK293 cells were incubated with forskolin (20 μM) for 6 h and harvested. Luciferase activity was measured in the lysates. Data represent the mean values ± s.e.m. from three independent experiments. Asterisks indicate statistically significant difference (*$P<0.001$, **$P<0.005$, and ***$P<0.05$ by one-way ANOVA). (**L**) The T93D FCoR mutant acetylates Foxo1 the most. After transfection with pFLAG-CMV2-WT Foxo1 with or without pCMV5-cMyc-WT (lane 4), T93A (lane 5), or T93D (lane 6) FCoR, HEK293 cells were incubated with (lanes 3–6) or without H_2O_2 (lanes 1 and 2) (500 μM), nicotinamide (NAM) (50 mM), and trichostatin A (TSA) (2 μM) for 3 h and harvested. Lysates were immunoprecipitated with anti-FLAG mouse monoclonal antibody (M2) and subjected to western blotting with the indicated antibodies. (**M**) Interaction between Foxo1 and FCoR. HEK293 cells were co-transfected with pCMV5-cMyc-Foxo1 and pFLAG-CMV2-WTFCoR and culture at the indicated condition. Cell lysates were immunoprecipitated with anti-FLAG, anti-cMyc or normal mouse IgG and blotted with anti-cMyc or anti-FLAG antibody. Figure source data can be found with the Supplementary data.

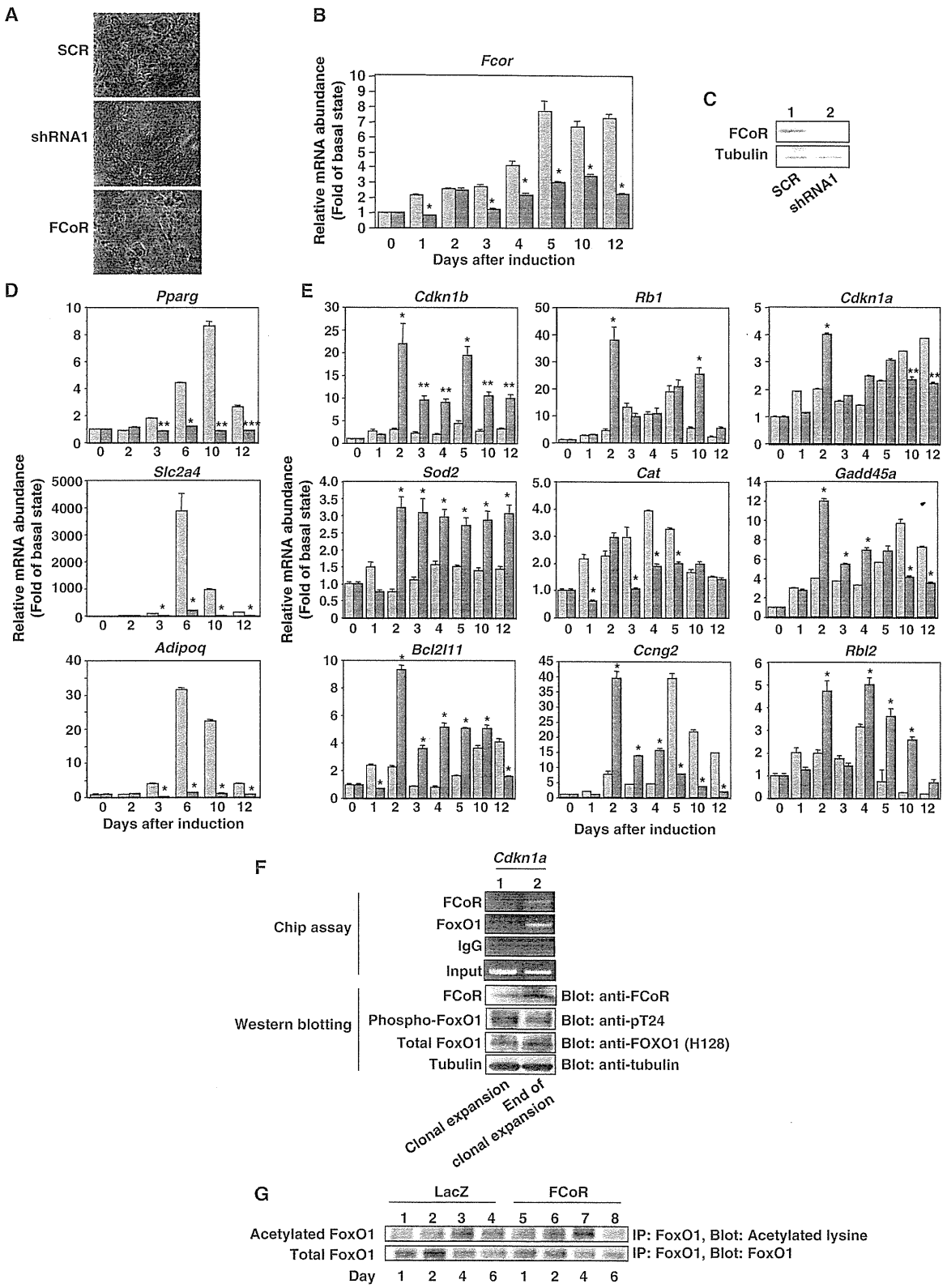

of FCoR in WAT inhibits the expression of Foxo1-target genes, decreases the size of adipocytes in WAT, and increases insulin sensitivity.

We crossed $Lepr^{db/+}$-*WFCoR* with $Lepr^{db/+}$ mice and generated $Lepr^{db/db}$-*WFCoR* mice in order to investigate whether overexpression of FCoR in WAT improves glucose metabolism in $Lepr^{db/db}$ mice. $Lepr^{db/db}$-*WFCoR* mice showed a significant decrease in body weight compared with $Lepr^{db/db}$ mice (Supplementary Figure S9A and B). IPGTT and ITT demonstrated that $Lepr^{db/db}$-*WFCoR* mice have improved glucose tolerance and insulin sensitivity (Supplementary Figure S9C and D). CT scans revealed decreased visceral fat mass in $Lepr^{db/db}$-*WFCoR* compared with $Lepr^{db/db}$ mice, despite similar total adipose tissue mass (Supplementary Figure S9E). Measurement of adipocyte size revealed that white adipocytes from $Lepr^{db/db}$-*WFCoR* mice were significantly smaller than those from $Lepr^{db/db}$ (Supplementary Figure S9F–H). Although the food intake and respiratory quotient of $Lepr^{db/db}$-*WFCoR* mice were similar to $Lepr^{db/db}$ mice, oxygen consumption was significantly increased (data not shown; Supplementary Figure S9I). Gene expression analysis demonstrated that the expression levels of *Ccl2* and several Foxo1-target genes were decreased significantly compared with levels in $Lepr^{db/db}$ mice (Supplementary Figure S9J–L). These data suggest that the FCoR in WAT can improve glucose metabolism in $Lepr^{db/db}$ mice.

We next examined the effects of overexpression of FCoR in mice with diet-induced obesity. The *WFCoR* mice had a lean phenotype compared with wild-type mice fed a HFD and had smaller adipocytes in WAT (Supplementary Figure S10A and B). IPGTT and ITT revealed that HFD *WFCoR* mice had improved glucose tolerance and insulin sensitivity compared with wild-type mice (Supplementary Figure S10C and D). These findings are in accordance with the idea that FCoR in WAT improves insulin sensitivity.

FCoR in BAT affects thermoregulation

We also analysed BAT function in *BFCoR* mice (Figure 6B–D). *BFCoR* mice have normal body weight (Supplementary Figure S11A) and IPGTT (Supplementary Figure S11B). Insulin sensitivity was similar to wild-type mice (Supplementary Figure S11C). We also measured oxygen consumption to investigate the effects of overexpression of FCoR on the physiological function of BAT. Oxygen consumption and the respiratory quotient of *BFCoR* mice were similar to wild-type mice (Supplementary Figure S11D and E). The *BFCoR* mice exhibited significantly reduced cold tolerance compared with wild-type mice (Figure 7A). We detected ~60% and ~50% decreases of *Ppargc1a* and *Ucp1*, respectively (Figure 7B), in *BFCoR* mice, along with a commensurate decrease in PGC-1α protein (Figure 7C). Furthermore, *BFCoR* mice exhibited reduced expression levels of mitochondrial components (Figure 7D). These data indicate that overexpression of FCoR in BAT suppresses thermoregulation by suppressing PGC-1α expression.

FCoR regulates PGC-1α gene expression

To examine whether FCoR can suppress *Ppargc1a* expression at the cellular level, we transduced the brown adipocyte cell line T37i cells with adenovirus encoding LacZ or cMyc-FCoR and examined endogenous *Ppargc1a* expression. Real-time PCR showed that overexpression of FCoR suppressed endogenous *Ppargc1a* expression in T37i cells in an FCoR dose-dependent manner (Figure 7E). The PGC-1α protein level was also decreased by FCoR expression in T37i cells (Figure 7F). To investigate whether FCoR suppresses *Ppargc1a* promoter activity, we performed a luciferase reporter assay using truncated versions of *Ppargc1a* promoters. The *Ppargc1a* promoter has two insulin-responsive elements, IRE1 and IRE2 (Figure 7G). To characterize the FCoR-target site in the *Ppargc1a*promoter, we constructed different versions of the mouse *Ppargc1a* promoter by progressively deleting portions of its upstream region. The transcriptional activity of each mutant promoter in response to FCoR was examined in T37i cells (Figure 7G). Mutant promoters with deletions up to −890 nt in the *Ppargc1a* promoter, which includes IRE1 and/or IRE2, still responded to FCoR. However, further deletion up to −483 nt, which has no IRE, completely abolished the

Figure 5 The effects of knockdown of FCoR on adipocyte differentiation. (**A**) Oil-red O staining of 3T3-F442A cells. At day 14 after induction of differentiation and transduction with adenoviruses encoding scrambled (the top panel), shRNA1 (the middle panel), and cMyc FCoR (the bottom panel), cells were stained with Oil-red O. (**B**) Knockdown of endogenous *Fcor* mRNA in 3T3-F442A cells during differentiation. 3T3-F442 cells were induced to differentiation into mature adipocytes as described in 'Supplementary Experimental Procedures' and transduced with adenovirus encoding shRNA1 (blue bar) or scrambled shRNA (grey bar). Total RNA was isolated from cells on the indicated day and subjected to real-time PCR of *Fcor* and β-*actin*. The data were corrected using the β-*actin* expression level and represent the mean values ± s.e.m. from two independent experiments. Asterisks indicate statistically significant differences between *Fcor* expression levels in scrambles- and shRNA1-transduced cells ($^*P<0.001$ by one-way ANOVA). (**C**) Western blotting of endogenous FCoR protein. On day 10 after transduction with adenovirus encoding scrambled or shRNA1, 3T3-F442A cells were harvested and the lysates were subjected to western blotting with the indicated antibodies. (**D**) Effects of knockdown of FCoR on the expression of adipocyte-specific genes during differentiation of 3T3-F442A cells. After induction of differentiation and transduction, total RNA was isolated on the indicated days and subjected to real-time PCR of *Pparg* (top panel), *Slc2a4* (middle panel), and *Adipoq* (bottom panel). The grey bar indicates scrambled-transduced cells and the blue bar indicates shRNA1-transduced cells. The data were corrected using the β-*actin* expression level and represent the mean values ± s.e.m. from two independent experiments. Asterisks indicate statistically significant difference between scrambled- and shRNA1-transduced cells ($^*P<0.001$, $^{**}P<0.005$, and $^{***}P<0.01$ by one-way ANOVA). (**E**) Effects of knockdown of FCoR on the expression levels of Foxo1-target genes during differentiation of 3T3-F442A cells. Total RNA from scrambled- (grey bar) or shRNA1-transduced cells (blue bar) on the indicated days was subjected to real-time PCR of the indicated Foxo1-target genes. The data were corrected using the β-*actin* expression level and represent the mean values ± s.e.m. from two independent experiments. Asterisks indicate statistically significant difference between scrambled- and shRNA1-transduced cells ($^*P<0.001$ and $^{**}P<0.005$ by one-way ANOVA). (**F**) Chromatin immuunoprecipitation (Chip) assay of the *Cdkn1a* promoter. The Chip assay was performed using 3T3-F442A cells during (lane 1) or at the end of clonal expansion (lane 2) with the indicated antibodies. The lower panel shows western blotting of 3T3-F442A cells lysates at the indicated period with the indicated antibodies. (**G**) Acetylation of endogenous Foxo1 in 3T3-F442A cells transduced with adenoviruses encoding LacZ (lanes 1–4) or cMyc-FCoR (lanes 5–8) during differentiation. After induction of differentiation and transduction, cells were harvested on the indicated day, immunoprecipitated with anti-FOXO1 antibody, and blotted with the indicated antibodies.

responsiveness of the mutant promoter to FCoR suppression (Figure 7G). Thus, the FCoR-target site was confined to a proximal in the mouse *Ppargc1a* promoter and FCoR suppressed *Ppargc1a* promoter activity. These data indicate that FCoR inhibits *Ppargc1a* expression. Using Chip assays, we investigated two IREs in the *Ppargc1a* promoter. Chip assays using both promoter regions revealed that FCoR bound the proximal IRE2 but not the distal IRE1 (Figure 7H). These data suggest that FCoR binds to the *Ppargc1a* promoter via IRE2.

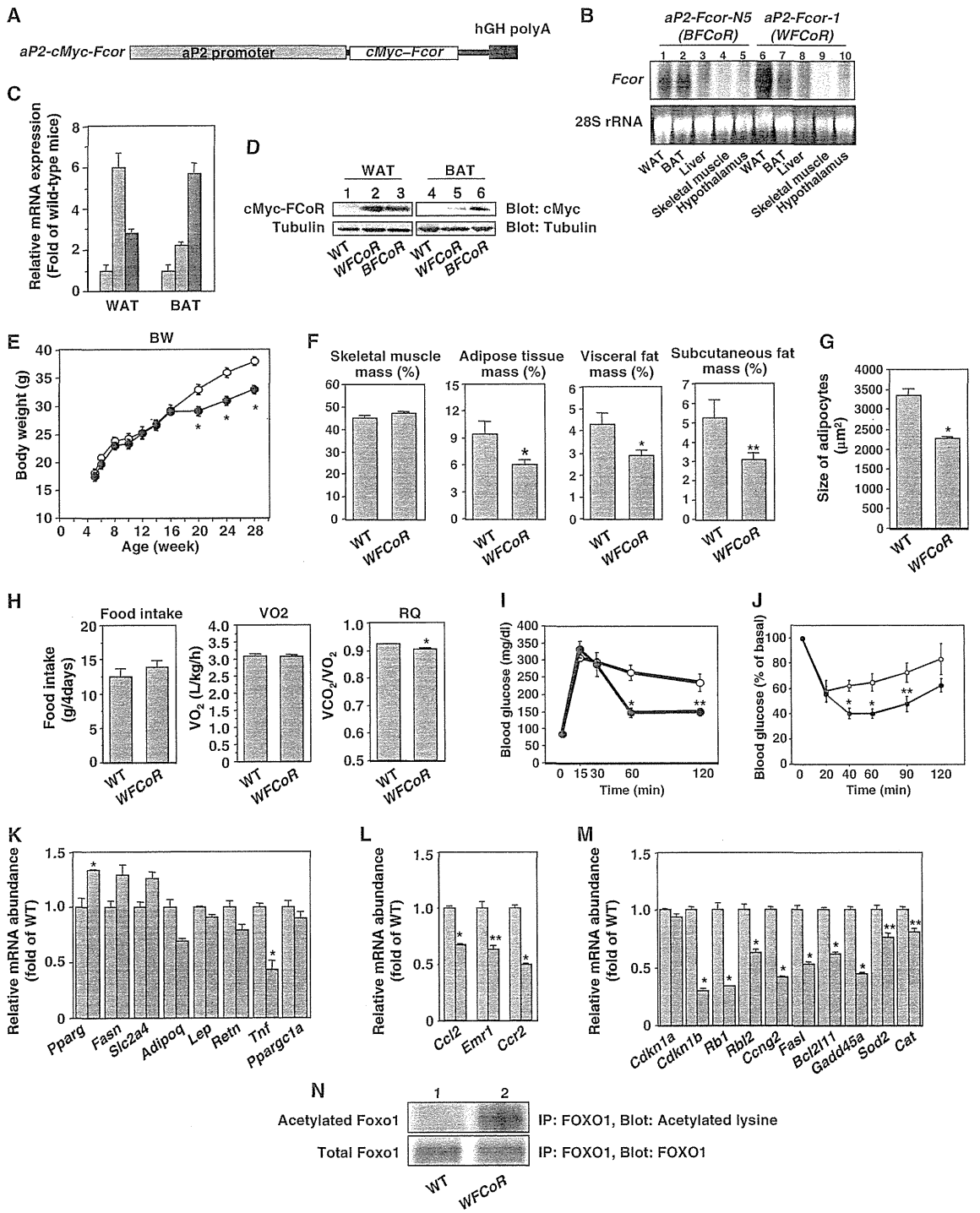

Fcor knockout mice exhibited insulin resistance

To investigate the physiological roles of FCoR, we generated *Fcor* knockout (*FcorKO*) mice (Supplementary Figure S12A–E). *FcorKO* mice had a lean phenotype, glucose intolerance, and insulin resistance on a normal chow diet (Figure 8A–C). CT scan revealed that *FcorKO* mice had adipose mass that was similar to that of WT mice, including the visceral and subcutaneous depots (data not shown). In contrast to our findings that FCoR is overexpressed in WAT, the size of epididymal fat adipocytes was larger in *FcorKO* mice than in wild-type mice (Figure 8D and E). These data suggest that there may be fewer adipocytes in *FcorKO* mice than in WT mice. The expression of several Foxo-target genes was significantly increased in both WAT and BAT in *FcorKO* mice (Figure 8F and G). The expression levels of WAT-specific genes were similar in *FcorKO* mice as in wild-type mice, but the expression levels of inflammatory genes, including *Emr1* and *Ccr2*, were significantly increased (Figure 8H and I), leading to insulin resistance (Olefsky and Glass, 2010).

Although the food intake of *FcorKO* mice was similar to that of wild-type mice, oxygen consumption was significantly increased and respiratory quotient was significantly decreased (Figure 8J–L). These data indicate that *FcorKO* mice had increased energy expenditure and increased usage of fat that led to a lean phenotype.

Overexpression of FCoR suppressed PGC-1α expression in *BFCoR* mice and T37i cells. Therefore, deletion of *Fcor* would be expected to increase PGC-1α expression. Indeed, the expression levels of *Ppargc1a* and the PGC-1α protein in the BAT of *FcorKO* mice were significantly increased compared with wild-type mice (Figure 8M and N). These data confirm that FCoR suppresses the transcriptional activity of Foxo1 and PGC-1α expression.

Discussion

Using a two-hybrid screen, we identified a Foxo1-CoRepressor termed as FCoR that is expressed in adipose tissue, inhibits Foxo1 transcriptional activity, and is phosphorylated by PKA and then translocated into the nucleus. FCoR is activated in a fasting or starved state, or during cold exposure, all conditions in which PKA is activated by glucagon or adrenergic stimuli. Thus, FCoR may be an important metabolic regulator that coordinates the insulin/cAMP response by interacting with Foxo. However, at fasting state, expression level of activated FCoR protein is decreased. We speculate that the active, presumed phosphorylated, FCoR protein is unstable and turned over rapidly.

Experiments showed that FCoR prevents Sirt1 binding to Foxo1, thus enhancing Foxo1 acetylation and inhibiting its transcriptional activity. Several proteins have been reported to affect Foxo1 and Sirt1. In *C. elegans*, two 14-3-3 proteins bind to SIR-2.1 and DAF-16 and are required for SIR-2.1-induced transcriptional activation of DAF-16 (Berdichevsky *et al*, 2006). Furthermore, four-and-a-half LIM 2 (FHL2) also interacts with FOXO1; FHL2 enhances the interaction between FOXO1 and SIRT1 and therefore enhances the deacetylation of FOXO1 (Yang *et al*, 2005). To date, FCoR is the only protein that is known to inhibit the interaction of Sirt1 and Foxo1.

Figure 6 Generation of transgenic mice expressing wild-type FCoR driven by the *aP2* promoter. (**A**) Diagram of the transgenic construct. In addition to 5.4 kb of the *aP2* promoter, the construct contains the *cMyc-WT Fcor* cDNA and the human *GH* polyadenylation sequences. (**B**) Tissue survey of transgene expression in WAT (lanes 1 and 6), BAT (lanes 2 and 7), liver (lanes 3 and 8), skeletal muscle (lanes 4 and 9), and hypothalamus (lanes 5 and 10) in line N5 (lanes 1–5) and line 1 (lanes 6–10). Total RNA was isolated from the tissues indicated at the bottom of the autoradiogram and analysed by northern blotting using *Fcor* or β-*actin* cDNA probe. (**C**) Real-time PCR of transgene expression in WAT and BAT from transgenic lines. Data represent the mean values ± s.e.m. of RNA samples from each of five transgenic mice for each tissue. The grey, sky blue, and red bars indicate wild-type, *aP2-FCoR-1* (*WFCoR*), and *aP2-FCoR-N5* (*BFCoR*), respectively. (**D**) Western blotting of transgenic cMyc-FCoR expression in WAT (lanes 1–3) and BAT (lanes 4–6). Lysates from the tissue of the indicated types of mice were subjected to western blotting with the indicated antibodies. (**E**) Body weight of wild-type and transgenic mice (*WFCoR*) fed a normal chow diet. Data represent the mean values ± s.e.m. of 15–20 male mice for each genotype. The open and closed circles indicate wild-type and *WFCoR* mice, respectively. An asterisk indicates a statistically significant difference between wild-type and *WFCoR* ($^*P<0.01$ by one-way ANOVA). (**F**) Adiposity of 5-month-old *WFCoR* transgenic mice fed a normal chow diet. Skeletal muscle mass, adipose tissue mass (sum of visceral and subcutaneous fat mass), visceral fat mass, and subcutaneous fat mass were calculated. The data are reported as percentage of body weight and represent the mean ± s.e.m. of five mice of each genotype. Asterisks indicate statistically significant differences between wild-type and *WFCoR* mice ($^*P<0.02$ and $^{**}P<0.05$ by one-way ANOVA). (**G**) Average of size of adipocytes from epididymal fat of 5-month-old wild-type (grey bar) and *WFCoR* (sky blue bar) mice fed a normal chow diet. An asterisk indicates a statistically significant difference between wild-type and *WFCoR* mice ($^*P<0.001$ by one-way ANOVA). (**H**) Food intake, oxygen consumption, and respiratory quotient of 5-month-old wild-type (grey bar) and *WFCoR* (sky blue bar) mice fed a normal chow diet. An asterisk indicates a statistically significant difference between wild-type and *WFCoR* mice ($^*P<0.001$ by one-way ANOVA). (**I**) Intraperitoneal glucose tolerance test in wild-type ($n=10$) and *WFCoR* transgenic mice ($n=10$) fed a normal chow diet. The open and closed circles indicate wild-type and *WFCoR* mice, respectively. Data represent the mean values ± s.e.m. Asterisks indicate statistically significant differences between wild-type and *WFCoR* mice ($^*P<0.005$ and $^{**}P<0.02$ by one-way ANOVA). (**J**) Intraperitoneal insulin tolerance test in wild-type ($n=8$) and *WFCoR* ($n=10$) mice fed a normal chow diet. Data represent the mean values ± s.e.m. Asterisks indicate statistically significant differences between wild-type and *WFCoR* mice ($^*P<0.005$ and $^{**}P<0.05$ by one-way ANOVA). (**K**) Real-time PCR of WAT-specific genes using WAT from wild-type (grey bar) and *WFCoR* transgenic mice (sky blue bar) fed a normal chow diet. Data represent the mean values ± s.e.m. of RNA samples from five mice of each genotype. An asterisk indicates a statistically significant difference between wild-type and *WFCoR* transgenic mice ($^*P<0.05$ by one-way ANOVA). (**L**) Real-time PCR of *Ccl2*, *Emr1*, and *Ccr2* genes using WAT from wild-type (grey bar) and *WFCoR* transgenic mice (sky blue bar) fed a normal chow diet. Data represent the mean values ± s.e.m. of RNA samples from five mice of each genotype. Asterisks indicate statistically significant differences between wild-type and *WFCoR* transgenic mice ($^*P<0.001$ and $^{**}P<0.005$ by one-way ANOVA). (**M**) Real-time PCR of Foxo1-target genes using WAT from wild-type (grey bar) and *WFCoR* transgenic mice (sky blue bar). Data represent the mean values ± s.e.m. of RNA samples from five mice of each genotype. Asterisks indicate statistically significant differences between wild-type and *WFCoR* transgenic mice ($^*P<0.001$ and $^{**}P<0.005$ by one-way ANOVA). (**N**) Acetylation of endogenous Foxo1 in WAT from 5-month-old wild-type (lane 1) and *WFCoR* transgenic mice (lane 2). Tissue lysates containing nicotinamide (NAM) (50 mM) and trichostatin A (TSA) (2 μM) were immunoprecipitated with anti-FOXO1 antibody and blotted with the indicated antibodies.

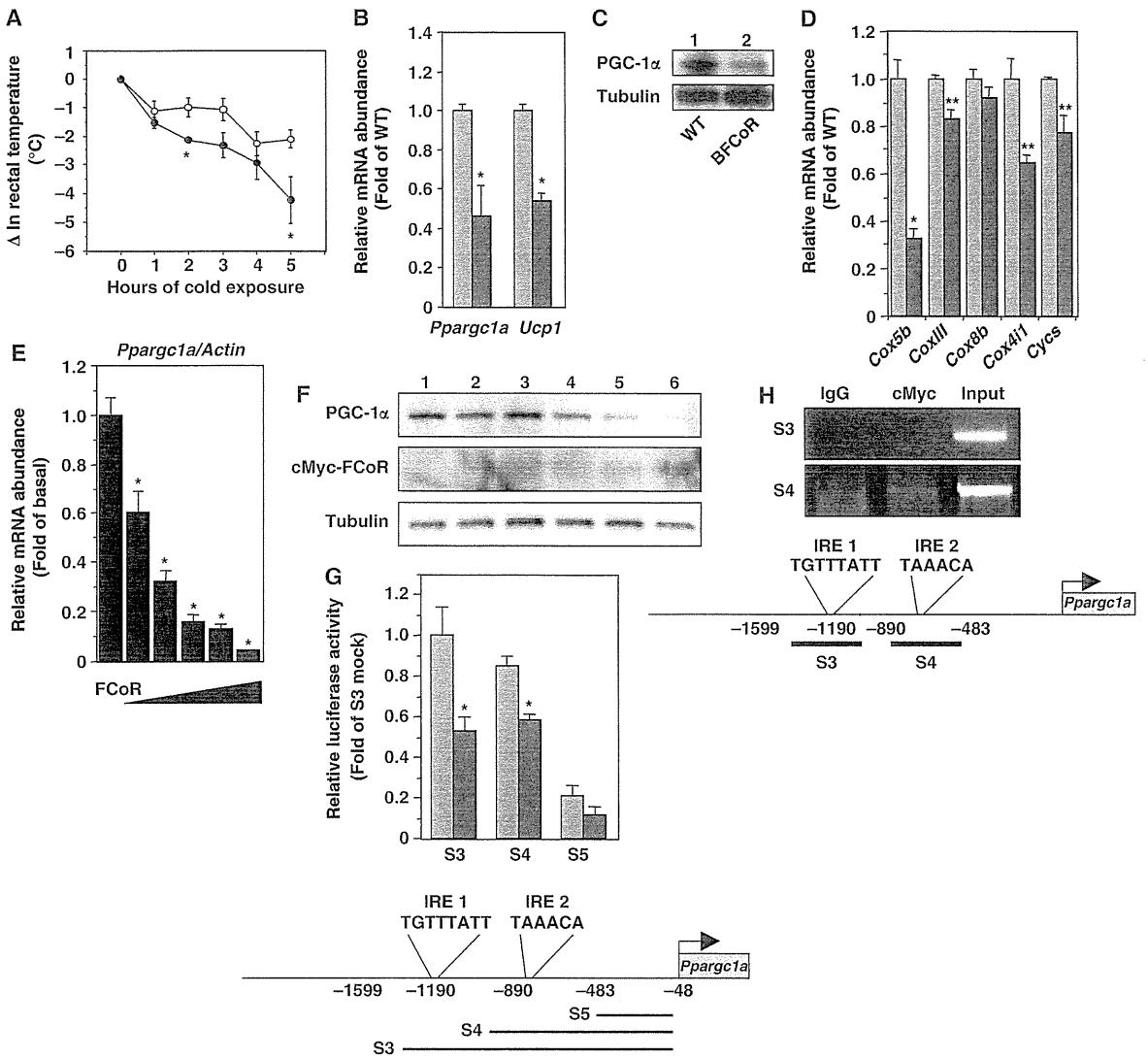

Figure 7 FCoR in BAT affects thermoregulation through suppression of *Ppargc1a* expression. (**A**) Changes in the rectal temperature of 6-month-old wild-type (open circle) and *BFCoR* (closed circle) mice after cold exposure. Data represent the mean values ± s.e.m. ($n=6$ for each genotype). Asterisks indicate statistically significant differences between wild-type and *BFCoR* transgenic mice ($^*P<0.05$ by one-way ANOVA). (**B**) Real-time PCR of *Ppargc1a* and *Ucp1* in BAT from wild-type (grey bar) and *BFCoR* transgenic mice (red bar). The data were corrected using the β-*actin* expression level and represent the mean values ± s.e.m. of three independent experiments ($n=6$ for each genotype). Asterisks indicate statistically significant differences between wild type and *BFCoR* transgenic mice ($^*P<0.05$ by one-way ANOVA). (**C**) Western blotting of PGC-1α and UCP-1 protein in BAT from wild-type (lane 1) and *BFCoR* transgenic mice (lane 2). Lysates (200 μg) of BAT from wild-type and *BFCoR* transgenic mice were subjected to western blotting with the indicated antibodies. (**D**) Real-time PCR of mitochondrial component genes using BAT from wild-type (grey bar) and *BFCoR* transgenic mice (red bar). Data represent the mean values ± s.e.m. of RNA samples from five mice of each genotype. Asterisks indicate statistically significant differences between wild-type and *BFCoR* transgenic mice ($^*P<0.001$ and $^{**}P<0.005$ by one-way ANOVA). (**E**) The effects of overexpression of cMyc-FCoR on endogenous *Ppargc1a* gene expression in T37i cells. T37i cells were transduced with adenovirus encoding LacZ or cMyc-FCoR. Cells were harvested 48 h after transduction. Total RNA was isolated and subjected to real-time PCR of *Ppargc1a*. Data were corrected using the β-*actin* expression level, shown as 'fold change' compared with LacZ-transduced cells, and represent the mean values ± s.e.m. from three independent experiments. An asterisk indicates a statistically significant difference between LacZ- and cMyc-FCoR-transduced cells ($^*P<0.001$ by one-way ANOVA). (**F**) PGC-1α protein expression was decreased in a dose-dependent manner by overexpression of FCoR in T37i cells. (**G**) Effect of FCoR on *Ppargc1a* promoter activity. Data were obtained in five experiments and are represented as the mean values ± s.e.m. of fold change compared with mock vector-transfected activity in T37i cells transfected with truncated *Ppargc1a* (S3). $^*P<0.001$ (one-factor ANOVA of cells transfected with pCMV5/cMyc and with pCVM5/cMyc-FCoR vector). (**H**) Chip assays of T37i cells transduced with an adenovirus encoding cMyc-FCoR and harvested 36 h after transduction. The PCR primers used to amplify the mouse *Ppargc1a* promoter sequence as indicated as S3 and S4. PCRss with total input chromatin are shown as controls. Figure source data can be found with the Supplementary data.

Recently, it has been reported that class IIa HDACs 4/5/7 and class I HDAC (HDAC3) are critical components of the transcriptional response to fasting in liver, shuttling into the nucleus in response to forskolin or glucagon. HDAC4 and 5 induces the acute transcription of gluconeogenic enzymes such as G6Pase via deacetylation and activation of Foxo family transcription factors (Mihaylova *et al*, 2011; Wang *et al* 2011). In the present study, we used trichostatin A (TSA) for the prevention of deacetylation of Foxo1. Therefore, we cannot exclude the possibility that FCoR works on the regulatory complex with the class IIa and I HDACs. It is established that in hepatocytes, Foxo is actively promoting transcription of its target genes after forskolin, glucagon, or cAMP treatment. However, *Fcor* is expressed little in liver of wild-type mice under normal chow diet. If FCoR is expressed in liver, then the predicted acetylation and inhibition of Foxo may run counter to the known activation of Foxo by forskolin/cAMP agonists.

Interestingly, FCoR itself has intrinsic acetyltransferase activity. Acetylation represents a fail-safe mechanism for preventing excessive Foxo1 activity (Banks *et al*, 2011). Therefore, FCoR may maintain Foxo1 acetylation by direct acetylation in the cytosol in the fed state and by interruption of the association of Foxo1 with Sirt1 in the nucleus in a fasting or starved state or during cold exposure. This is consistent with the idea that FCoR acts to fine-tune Foxo1 activity (Figure 9). FCoR can also acetylate other transcription factors and cofactors (Nakae *et al*, unpublished observation). Therefore, the sudden decline of body weight in *WFCoR* mice may be due to acetylation of other binding partners of FCoR. Further investigation of FCoR-binding proteins is needed to identify such partners.

The finding that knockdown of endogenous FCoR inhibited the differentiation of 3T3-F442A cells suggests that FCoR is indispensable for adipocyte differentiation. This is in keeping with our previous findings that overexpression of CN Foxo1 (ADA) inhibits the differentiation of 3T3-F442A cells (Nakae *et al*, 2003). Jing *et al* reported that the KR mutant of Foxo1, which is activated and thus mimics the deacetylated protein (Banks *et al*, 2011), inhibits adipocyte differentiation (Jing *et al*, 2007). Therefore, knockdown of FCoR may accelerate Foxo1 deacetylation and so inhibit adipogenesis.

The present study demonstrated that while FCoR overexpression decreased the adipocyte size in transgenic mice, *FcorKO* mice exhibited increased adipocyte size, consistent with findings for Foxo1 haploinsufficiency or transgenic mice overexpressing a dominant-negative Foxo1 mutant in fat cells (*aP2-FLAG-Δ256*) (Nakae *et al*, 2003, 2008a; Kim *et al*, 2009). Namely, inhibition of Foxo1 leads to smaller adipocytes. Therefore, inhibition of Foxo1 by overexpression of FCoR reduces adipocyte size. On the other hand, activation of Foxo1 by deletion of FCoR increases adipocyte size. Foxo1 is involved in the early stages of adipose conversion (Nakae *et al*, 2003). Therefore, it is speculated that generation of adipocytes in *FcorKO* mice is decreased due to activation of Foxo1. Previous reports showed that Foxo1 inhibits PPARγ activity (Dowell *et al*, 2003; Armoni *et al*, 2006; Fan *et al*, 2009). Knockdown of FCoR should enhance Foxo1 activity, leading to inhibition of PPARγ and adipogenesis. However, in the present study, FCoR did not prevent Foxo1-induced inhibition of PPARγ activity. More than that, knockdown of *Fcor* suppressed *Pparg* gene expression in 3T3-F442A cells and overexpression of FCoR in WAT significantly increased *Pparg* expression. Foxo1 represses transcription from either *Pparg1* or *Pparg2* promoter (Armoni *et al*, 2006). Therefore, inhibition of Foxo1 by FCoR may work on *Pparg* promoter and increase *Pparg* expression, leading to enhanced adipogenesis and smaller adipocytes.

We found that FCoR expression in BAT of transgenic mice led to cold intolerance and to decreased expression levels of *Ppargc1a* and *Ucp1*, suggesting that FCoR regulates brown adipocyte function. FCoR expression is induced by cold exposure. Therefore, FCoR in BAT may restrict mitochondrial biogenesis during cold exposure by inhibition of *Ppargc1a* expression. However, the findings are inconsistent with our previous report that *aP2-FLAG-Δ256* mice, in which a transactivation-defective Foxo1 (Δ256) is expressed in both WAT and BAT, showed increased oxygen consumption accompanied by increased expression of PGC-1α, uncoupling protein (UCP)-1, UCP-2, and β3-adrenergic receptor (β3-AR) (Nakae *et al*, 2008a). If FCoR works by inhibiting Foxo1 activity in BAT, then overexpression of FCoR should enhance the thermogenic function of BAT, leading to increased expression of *Ppargc1a* and increased energy expenditure. Therefore, FCoR may inhibit *Ppargc1a* expression via other partners but not via inhibition of Foxo1 in BAT. However, in liver, *Ppargc1a* is a transcriptional target that is induced by the dephosphorylation mutant of Foxo1 (Daitoku *et al*, 2003; Matsumoto *et al*, 2006). Further investigation is needed to clarify the molecular target of FCoR in the *Ppargc1a* promoter in BAT.

FCoR acts as a 'repressor' of Foxo1 and Foxo3a but not of Foxo4. The failure to identify homologous genes in *C. elegans*, along with the repression of FCoR expression in states of food deprivation, indicates that FCoR may act as an anti-thrifty gene. FCoR regulates insulin sensitivity by altering the size of white adipocytes in WAT and induces cold intolerance by inhibiting *Ppargc1a* expression. FCoR is thus an attractive therapeutic target for treatment of obesity and type 2 diabetes.

Materials and methods

Antibodies and cell cultures

Anti-FCoR antisera were raised by immunizing rabbits with a peptide corresponding to amino acids 2–16 of the mouse FCoR sequence (GGPTRRHQEEGSAEC). Phospho-threonine 93 rabbit polyclonal antibodies (anti-pT93) were produced by immunizing rabbits with a synthetic phosphorylated peptide coupled to KLH that corresponded to amino acids 85–94 surrounding mouse FCoR Threonine 93 (LDLNSQRS-T (PO_3H_2)-C). Antibodies were purified using Activated Thiol-Sepharose 4B (Pharmacia) Peptide Columns and peptide affinity chromatography (TAKARA BIO, Inc.). We purchased anti-FLAG (M2) and anti-tubulin from Sigma; anti-cMyc (9E10), anti-FOXO1 (H128), anti-PGC-1 (H300), and anti-GST (Z-5) from Santa Cruz Biotechnology; and anti-phospho-FOXO1 (pT24), and anti-acetylated lysine polyclonal antibodies from Cell Signaling Technology. HEK293 cells and T37i cells were cultured as described previously (Nakae *et al*, 1999, 2008a). Preadipocytes cell line 3T3-F442A cells were cultured and induced differentiation into mature adipocytes as described previously (Nakae *et al*, 2003). Staining 3T3-F442A cells with oil red O was described previously (Nakae *et al*, 2003).

Yeast two-hybrid screen

Amino acids 1–154 of murine Foxo1 were cloned in-frame into the GAL4 DNA-binding domain plasmid pGBKt7 (Clontech). The GAL4 activation domain 3T3-L1 cDNA library of 3T3-L1 was the kind gift of Dr Alan R Saltiel (University of Michigan Medical Center, Michigan, USA) (Printen *et al*, 1997). The AH109 yeast strain was used for the library search. The transformation was performed as described in the

Clontech Matchmaker two-hybrid system 3 protocol. The transformants were plated on SD/-Ade/-His/-Leu/-Tyr plates in the presence of galactose and then were incubated at 30°C for 3–4 days. Positive interaction was identified by strong β-galactosidase activity. Individual positive clones were isolated using the Yeastmaker yeast plasmid isolation kit (BD Bioscience), sequenced by an ABI310 automated DNA sequencer, and analysed for homology with sequences in the GenBank database using the BLAST algorithm.

Rapid amplification of cDNA ends

In order to determine the complete 5′ and 3′ sequence of *Fcor* mRNA, we performed both 5′- and 3′-RACE using the SMART RACE cDNA Amplification Kit (Clontech) according to manufacturer's protocol. In brief, we isolated total RNA from the WAT and BAT of wild-type mice and synthesized first-strand cDNA. After that, we performed 5′- and 3′-RACE PCR using the following gene specific primers: 5′-CACCACTACCATCACCACACTGCACCGG-3′ for 5′-RACE

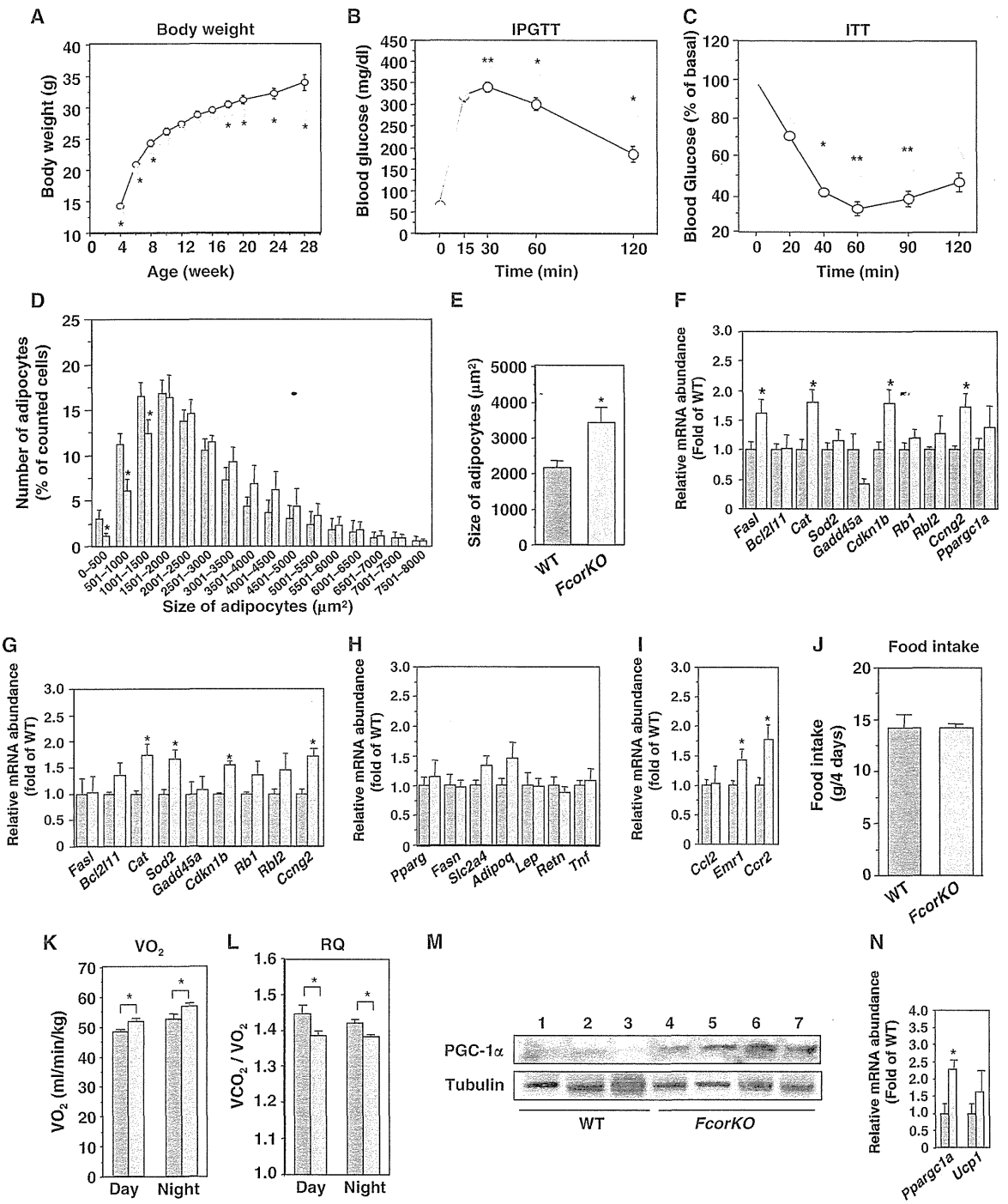

PCR and 5′-CCCCGGGTTTGCAAGGATGGATGGGAATG-3′ for 3′-RACE PCR. The PCR products were separated by electrophoresis in a 1.5% agarose gel (Supplementary Figure 1B). After purification using the QIAquick^{R} Gel Extraction Kit (QIAGEN), PCR products were subcloned into the pCRII^{R} vector (Invitrogen) using the TA Cloning Kit^{R} (Invitrogen) and sequenced.

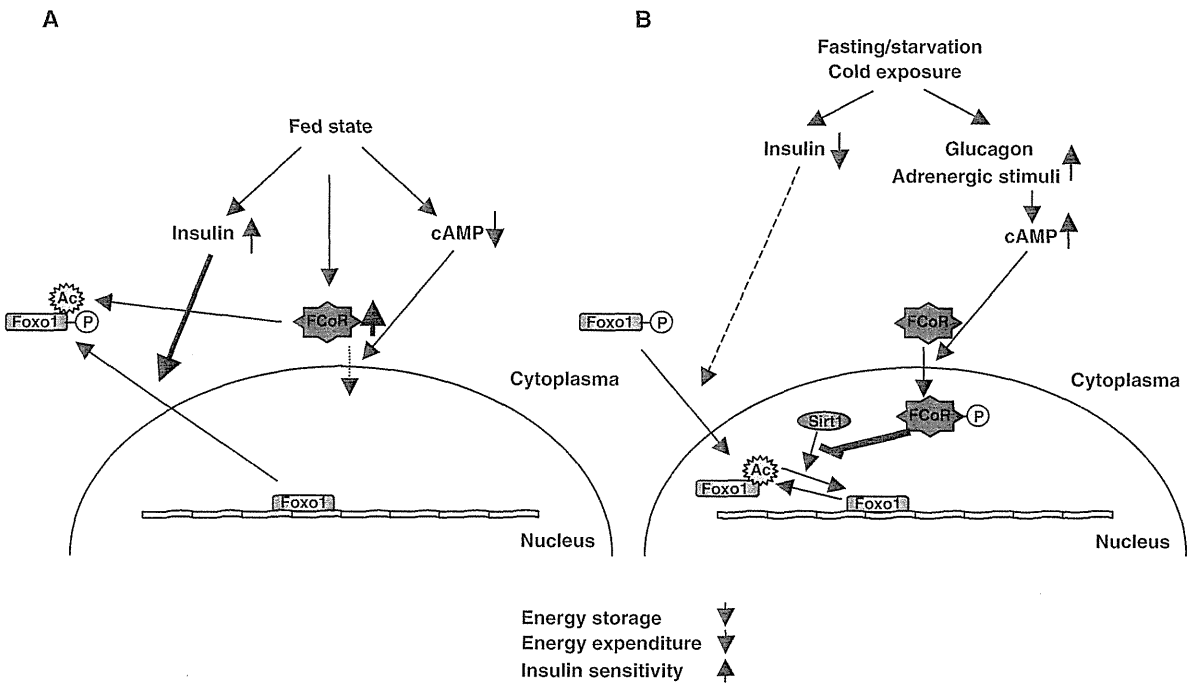

Figure 9 A model for the roles of FCoR in fine-tuning of Foxo1 activity. (**A**) When mice are in the fed state, Foxo1 is phosphorylated and FCoR expression is increased. Both proteins remain in the cytosol. FCoR acetylates Foxo1 directly and keeps it in the acetylated state. (**B**) When mice are in the fasting state, insulin level decreases and Foxo1 remains in the nucleus and is activated. At the same time, glucagon from pancreatic α-cells is increased and activates cAMP-dependent protein kinase (PKA). Furthermore, upon exposure to the cold, adrenergic stimuli also activate PKA. These events lead to the nuclear localization of FCoR, which increases acetylation of Foxo1 by interrupting the association between Foxo1 and Sirt1. FCoR thus regulates energy storage, energy expenditure, and insulin sensitivity by fine-tuning Foxo1 function.

Figure 8 Deletion of *Fcor* induces insulin resistance. (**A**) Body weight of wild-type and *FcorKO* mice fed a normal chow diet. Data represent the mean values ± s.e.m. of 20–30 male mice for each genotype. The open and yellow closed circles indicate wild-type and *FcorKO* mice, respectively. An asterisk indicates statistically significant difference between wild-type and *FcorKO* (*$P<0.01$ by one-way ANOVA). (**B**) Intraperitoneal glucose tolerance test in wild-type ($n=10$) and *FcorKO* mice ($n=10$) under normal chow diet. The open and yellow closed circles indicate wild-type and *FcorKO* mice, respectively. Data represent mean values ± s.e.m. Asterisks indicate statistically significant differences between wild-type and *FcorKO* mice (*$P<0.001$ and **$P<0.02$ by one-way ANOVA). (**C**) Intraperitoneal insulin tolerance test in wild-type ($n=10$) and *FcorKO* ($n=10$) fed a normal chow diet. Data represent the mean values ± s.e.m. Asterisks indicate statistically significant differences between wild-type and *FcorKO* mice (*$P<0.005$ and **$P<0.05$ by one-way ANOVA). (**D**) Distribution of adipocyte size. The sizes of single adipocytes from 5-month-old wild-type (grey bar) or *FcorKO* (yellow bar) mice fed a normal chow diet were measured as described in 'Supplementary Experimental Procedures'. The data represent the mean values ± s.e.m. of the percentage of all adipocytes with the indicated size. Asterisks indicate statistically significant differences between wild-type and *FcorKO* mice (*$P<0.05$ by one-way ANOVA). (**E**) The average of size of adipocytes from (**D**). An asterisk indicates a statistically significant difference between wild-type and *FcorKO* mice (*$P<0.005$ by one-way ANOVA). (**F, G**) Real-time PCR of Foxo1-target genes using WAT (**F**) and BAT (**G**) from wild-type (grey bar) and *FcorKO* (yellow bar) mice. Data represent the mean ± s.e.m. of RNA samples from 10 mice of each genotype. Asterisks indicate statistically significant differences between wild-type and *WFCoR* transgenic mice (*$P<0.05$ by one-way ANOVA). (**H**) Real-time PCR of WAT-specific genes using WAT from wild-type (grey bar) and *FcorKO* (yellow bar) mice fed a normal chow diet. Data represent the mean values ± s.e.m. of RNA samples from five mice of each genotype. (**I**) Real-time PCR of *Ccl2*, *Emr1*, and *Ccr2* genes using WAT from wild-type (grey bar) and *FcorKO* (yellow bar) mice. Data represent the mean values ± s.e.m. of RNA samples from five mice of each genotype. Asterisks indicate statistically significant differences between wild-type and *FcorKO* mice (*$P<0.05$ by one-way ANOVA). (**J**) Food intake of 5-month-old wild-type (grey bar) and *FcorKO* (yellow bar) mice. Data represent the mean values ± s.e.m. of food intake for 4 days. (**K, L**) The effects of deletion of *Fcor* on energy expenditure. Average oxygen consumption (**K**) and respiratory quotient (**L**) of 5-month-old wild-type (grey bar) and *FcorKO* (yellow bar) mice fed a normal diet. Data represent the mean values ± s.e.m. of six male mice for each genotype. Measurements of oxygen consumption were performed for 72 h after allowing the mice to acclimate to the cage environment. An asterisk indicates a statistically significant difference between wild-type and *FcorKO* mice (*$P<0.05$ by one-way ANOVA). (**M**) Western blotting of PGC-1α (top panel) and tubulin (bottom panel) in BAT from wild-type (lanes 1–3) and *FcorKO* (lanes 4–7) mice. (**N**) Real-time PCR of *Ppargc1a* and *Ucp1* using BAT from wild-type (grey bar) and *FcorKO* (yellow bar) mice. Data represent the mean values ± s.e.m. of RNA samples from 10 mice of each genotype. Asterisks indicate statistically significant differences between wild-type and *WFCoR* transgenic mice (*$P<0.05$ by one-way ANOVA). Figure source data can be found with the Supplementary data.

RNA isolation, real-time PCR, and northern blotting

Isolation of total RNA from tissues and cells was performed using the SV Total RNA Isolation System (Promega) according to manufacturer's protocol. Real-time PCR was performed as described previously (Nakae *et al*, 2008a). The primers used in this study are described in Table S1. We used the following primers for amplification of *Fcor*: 5′-ATGGGCGGTCCTACACGCCGCCAT-3′ (sense) and 5′-CTAGCACATGCCTTTAGTCCC-3′ (antisense). Northern blotting was performed using standard techniques. To prepare the probe for *Fcor*, we performed PCR using pCMV5/cMyc-FCoR plasmid as a template and the same primers as in real-time PCR. The probe used here for β-*actin* was described previously (Nakae *et al*, 2008a).

Construction of expression vectors

To construct pCMV5/cMyc-FCoR, we reverse transcribed total RNA from mouse BATs using the GeneAmpR RNA PCR Core Kit (Applied Biosystems) and performed PCR using the following primers: 5′-GG TCTAGA (*Xba*I) ATGGGCGGTCCTACACGCCGC-3′ (FCoR-S) and 5′-GG TCTAGA (*Xba*I) CTAGCACATGCCTTTAGTCCC-3′ (FCoR-AS). After treatment with *Xba*I, PCR products were subcloned into the *Xba*I-treated pCMV5/cMyc vector (Nakae *et al*, 1999). To construct pFLAG-CMV2-FCoR, we performed PCR using pCMV5/cMyc-FCoR as a template and FCoR-S and FCoR-AS as primers. *Xba*I-treated PCR products were subcloned into *Xba*I-treated pFLAG-CMV2 vector. To construct pFLAG-CMV2-WT FoxO1, *Xba*I-treated WT-FoxO1 fragments from pCMV5/cMyc-WT FoxO1 vector were subcloned into *Xba*I-treated pFLAG-CMV2 vector. Construction of pCMV5/cMyc-WT FoxO3a was described previously (Takaishi *et al*, 1999; Nakae *et al*, 2001). To construct pCMV5/cMyc-WT FOXO4, human FOXO4 cDNA was amplified by PCR using PFN21AB7772 (Kazusa DNA Research Institute, Chiba, Japan) and the following primers: 5′-GGG *ATCGAT* (*Cla*I) ATGGATCCGGGGAATGAGAAT-3′ (sense) and 5′-GGG *AAGCTT* (*Hin*dIII) TCAGGGATCTGGCT CAAAGTT-3′ (antisense). After treatment with *Cla*I and *Hin*dIII, PCR products were subcloned into *Cla*I/*Hin*dIII-treated pCMV5/cMyc vector. All vectors produced for this study were sequenced to confirm that they had the intended sequences.

Site-directed mutagenesis

Site-directed mutagenesis was carried out using the QuickChange^{R}II Site-Directed Mutagenesis Kit (Stratagene). We used the pCMV5/cMyc-FCoR expression vector as a template. To construct S92A-FCoR, we used the following mutagenic primers: S92A-S 5′-gaa ctcacaaagaGccacctgctgctgcct-3′ and S92A-AS 5′-aggcagcagcaggtgg Ctctttgtgagttc-3′. To construct T93A-FCoR, we used T93A-S 5′-gaac tcacaaagatccGcctgctgctgcct-3′ and T93A-AS 5′-aggcag cagcaggCgga tctttgtgagttc-3′. To construct T93D-FCoR, we used T93D-S 5′-gaactc acaaagatccGActgctgctgcct-3′ and T93D-AS 5′-aggcagcagcagTCggat ctttgtgagttc-3′. To construct S92A/T93D-FCoR, we used S92A/T93A-S 5′-gaactcacaaagaGccGcctgctgctgcct-3′ and S92A/T93A-AS 5′-aggcagcagcaggCggCtctttgtgagttc-3′. To construct I78A-FCoR, we used I78A-S 5′-ctacagagccctggctctGCtggaactctatatatcagg-3′ and I78A-AS 5′-cctgatatatagagttccaGCagagccagggctctgtag-3′. To construct T80A-FCoR, we used T80A-S 5′-ccctggctctattggagctctatatatcaggctgg-3′ and T80A-AS 5′-ccagcctgatatatagagctccaatagagccaggg-3′. To construct L81A-FCoR, we used L81A-S 5′-cctggctctattggaa ctGCatatatcaggctggacttg-3′ and L81A-AS5′-caagtccagcctgatatatGC agttccaatagagccagg-3′. To construct L85A-FCoR, we used L85A-S 5′-ggaactctatatatcaggGCggacttgaactcacaaaga-3′ and L85A-AS5′-tctttgtgagttcaagtccGCcctgatatatagagttcc-3′. To construct L87A-FCoR, we used L87A-S 5′-ctatatatcaggctggacGCgaactcacaa agatccacc-3′ and L87A-AS5′-ggtggatctttgtgagttcGCgtccagcctgatata tag-3′.

Construction of adenoviral vectors and adenoviral transduction

To construct an adenoviral vector encoding FCoR, we amplified the cMyc-FCoR cDNA fragment using the pCMV5/cMyc-FCoR expression vector as a template and the following primers: 5′- GG *GCTAGC* (*Nhe*I) ATGGAGCAGAAGCTGATCAGC-3′ (sense) and 5′-GG *GCTAGC* (*Nhe*I) CTAGCACATGCCTTTAGTCCC-3′ (antisense). After treatment with *Nhe*I, the PCR fragment was subcloned into *Nhe*I-treated pShuttle2 vector (Clontech). After sequencing the vectors to confirm that they had the intended sequences, and confirming protein expression in HEK293 by transient transfection, an I-CeuI- and PI-SceI-treated fragment was subcloned into Adeno-X viral DNA (pAdeno-X-cMyc-FCoR) (Clontech). The adenovirus vector was generated by transfecting HEK293 cells with the pAdeno-X-cMyc-FCoR plasmid.

For knockdown of FCoR in 3T3-F442A cells, we used DNA-based adenoviral vector-mediated technology (Knockout RNAi Systems; Clontech Laboratories, Inc.), with 5′-GCATGTGCTAGCATGCATA GC-3′ and 5′-GCTAGCATGCATAGCCTAATG-3′ as the targeted sequences of shRNA1 and shRNA2, respectively. The sequences of shRNA1 and shRNA2 are 5′-GATCCG GCATGTGCTAGCATGCATAGC TTCAAGAGA GCTATGCATGCTAGCACATGC CTTTTTT TCTAGA G-3′ and 5′-GATCCG GCTAGCATGCATAGCCTAATG TTCAAGAGA CATTAGGCTATGCATGCTAGC CTTTTTT TCTAGA G-3′, respectively. We selected an RNAi target sequence for FCoR using the Block-iT RNAi Designer (Invitrogen). We used the BD Adeno-X Expression System 1 (BD Biosciences) to generate a recombinant adenovirus encoding FCoR-shRNA. The generation of adenovirus encoding the cCN Foxo1 (T24A/S253A/S316A) was described previously (Nakae *et al*, 2006). For induction of endogenous *Igfbp1*, SV40-transformed hepatocytes were transduced with adenovirus encoding CN Foxo1 as described previously (Nakae *et al*, 2006). For transduction of 3T3-F442A cells with adenovirus encoding FCoR-shRNA, 3T3-F442A cells were transduced with adenovirus as described previously (Nakae *et al*, 2003).

Western blotting and fractionation of cytoplasmic and nuclear proteins

We homogenized tissues and lysed cells in buffer containing 50 mM Tris–HCl (pH 8.0), 250 mM NaCl, 1% NP-40, 0.5% deoxycholate, 0.1% SDS, and protease inhibitors (Roche Diagnostics). After centrifugation to remove insoluble material, the proteins in 30 μg of lysate were separated using 8 or 14% SDS–PAGE, and western blotting was performed using the indicated antibodies. Immunoprecipitation was performed as described previously (Cao *et al*, 2006). Fractionation of cytoplasmic and nuclear extracts was performed using NE-PER extraction reagents (Pierce). Protein concentrations in the cytoplasmic and nuclear extracts were determined using the Micro BSA protein assay kit (Pierce), and the proteins in aliquots (30 μg) were resolved by 14% SDS–PAGE followed by western blotting using the indicated antibody.

Detection of phosphorylated FCoR protein

For detection of phosphorylated FCoR, HEK293 cells were transfected with the indicated vectors encoding cMyc-FCoR. Cells were stimulated with forskolin (20 μM) for the indicated time and harvested using lysis buffer containing phosphatase inhibitor as described previously (Nakae *et al*, 2000). The proteins in the cell lysates were separated by 14% SDS–PAGE and transferred onto Immobilon-P Transfer Membrane (Millipore Corporation). After blocking, the membrane was incubated with *Phos-tag*^{R} BTL-104 (NARD Institute Ltd.) according to manufacturer's protocol followed by detection with streptavidin-horseradish peroxidase conjugate (ECL; Amersham, Buckinghamshire, UK). The membranes were reprobed as per manufacturer's protocol.

In-vitro translation and glutathione S-transferase fusion protein pull-down assay

The wild-type *Fcor* cDNA fragment was generated by PCR using pCMV5/cMyc-FCoR expression vector as a template and the following primers: 5′-GG GAATTC (*Eco*RI) GGATGGGCGGTCCTACACGC CGCCAT-3′ (sense) and 5′-GG GAATTC (*Eco*RI) CTAGCACATGCC TTTAGTCCC-3′ (antisense). The fragment was cloned in-frame into the *Eco*RI site of pGEX-4T-2. *In-vitro* translation of Foxo1 and the pull-down assay were performed as described previously (Cao *et al*, 2006).

In-vitro acetylation assay

GST-Foxo1-C1 fusion protein (20 μg) was incubated at 30°C for 1 h with 4 μg of GST, GST-FCoR fusion protein, or 0.5 μg of recombinant p300 protein (ACTIVE MOTIF) and 25 nCi of [^{14}C] acetyl-CoA (Perkin-Elmer) in the reaction buffer (50 mM Tris–HCl (pH 8.0), 100 mM NaCl, 10% glycerol, 0.1 mM EDTA, 1 mM DTT, 1 mM PMSF, 5 mM sodium butyrate). Reaction products were separated by 14% SDS–PAGE, stained with Coomassie brilliant blue, dried, exposed to a BAS 5000 imaging plate (FujiFilm, Japan) and analysed.

In-vitro phosphorylation assay

Five micrograms of GST, GST-WT FCoR, GST-T93A, GST-T93D, and GST-RRAS as a positive control (GST-RRAS is a short sequence of salt-inducible kinase (SIK) 2 and a substrate of PKA) were incubated at 30°C for 10 min with 0.5 units of the catalytic subunit of cAMP-dependent protein kinase (Promega) in the reaction buffer (50 mM Tris–HCl (pH 7.4), 0.1 mM DTT, 5 mM $MgCl_2$, 0.5 mM ATP). Reaction products were separated by 14% SDS–PAGE and transferred onto a nylon membrane. Phosphorylated products were detected using *Phos-tag*^{R} BTL-104 as described above and then blotted with anti-GST antibody.

Generation of adipose tissue-specific FCoR transgenic mice

We cloned wild-type *Fcor* cDNA into the *Sma*I site of plasmid pCMV5-aP2, into which the *Cla*I- and *Sma*I-treated 5.4-kb promoter-enhancer fragment of the mouse aP2 gene was subcloned into the *Cla*I/*Sma*I-treated pCMV5/cMyc vector (Nakae *et al*, 2008a). We excised the transgene with *Cla*I and *Xho*I, gel-purified it and injected it into fertilized eggs from BDF1 X C57BL/6 mice. The resulting embryos were implanted into CD-1 foster mothers. We screened the offspring for transgene transmission by PCR. Of 11 independent transgenic lines obtained, 9 founders transmitted the transgene through the germ line. We crossed each founder with C57BL/6 mice, obtained F1 mice, sacrificed one of the mice in each line in which transgene was transmitted and examined transgene expression in adipose tissues. We obtained three independent *Fcor* transgenic lines (Acc. No. CDB0446T: http://www.cdb.riken.jp/arg/TG%20mutant%20mice%20list.html) in which the transgene was expressed in adipose tissues. Primers for genotypying are 5′-ATG GAG CAG AAG CTG ATC AGC-3′ and 5′-CAT CCT TTC TCT GTG ATA CTG-3′.

Generation of FcorKO

The mouse genomic DNA clone containing exons 1 and 2 of the *Fcor* gene was obtained from a genomic DNA library derived from the 129/Sv mouse strain. The *Fcor* targeting construct consisted of 5.5 kb of genomic sequence that was immediately 5′ of the first exon, followed by a 4.5-kb LacZ-cassette, a Neo-resistance gene, and 3.5 kb of genomic sequence from intron 1, exon 2, and intron 2. The *Spe*I-linearized targeting vector was electroporated into TT2 embryonic stem (ES) cells (Yagi *et al*, 1993) as described previously. G418-resistant clones were isolated and screened by PCR and Southern blotting. In all, 30 out of 115 G418-resistant clones had undergone the desired homologous recombination. Positive clones were injected into CD-1 8-cell stage embryos, and the chimeric male offspring was mated to C57BL/6 females. Mice carrying the mutation in the heterozygous state were intercrossed to produce homozygous *Fcor* mutants (Acc. No. CDB0612K: http://www.cdb.riken.jp/arg/mutant%20mice%20list.html), and 20- to 24-week-old mice were used for analysis. Primers for detection of wild-type allele (204 bp) are 5′-ATGGGCGGTCCTACACGCCGC-3′ and 5′-CGGTGCAGTTCCCAGCCCTAC-3′. Primers for detection of knockout allele (234 bp) are 5′-AGCCCTTCCCCGCTGTGCACG-3′ and 5′-GGGTTTTCCCAGTCACGACGT-3′.

Animal studies, analytical procedures, IPGTT, and ITT

We used only male mice for the following experiments, as they are more susceptible to insulin resistance and diabetes. Animals were fed a standard chow diet and water *ad libitum* in sterile cages in a barrier animal facility with a 12-h/12-h light/dark cycle. Wild-type littermates were used as controls. All experimental protocols using mice were approved by the animal ethics committee of the Keio University School of Medicine and Kobe University Graduate School of Medicine. A HFD was started at weaning (4 weeks of age) and continued for 20 weeks. We used the same HFD and measured the blood glucose and insulin levels as described previously (Nakae *et al*, 2008a). We carried out all assays in duplicate. Each value represents the mean of two independent determinations. Glucose, ITT, and CT scanning were performed as described previously (Nakae *et al*, 2008a). The rectal temperature of mice was measured using Thermal Sensor^R (Shibaura Electronics Co. Ltd).

Luciferase assay

The IGFBP-1 or G6Pase luciferase assay was performed as described previously (Nakae *et al*, 2006). To construct a mouse *Ppargc1a* promoter-luciferase vector, mouse genomic DNA was amplified by PCR using the following primers: 5′-GG GCTAGC (*Nhe*I) TCATTGACTCAGGAACGACA-3′ (forward primer) and 5′-GG GCT AGC (*Nhe*I) CCAGTCACATGACAAAGCTA-3′ (antisense primer). After digestion with *Nhe*I, the PCR product was subcloned into *Nhe*I-treated pGL3-Basic vector (Promega) and sequenced to rule out the presence of mutations. For the mouse *Ppargc1a* promoter luciferase assay, HEK 293 cells were plated onto 12-well culture dishes. Transfections were carried out on cells at a 70–80% stage of confluence using 1.5 μg of pGL3/Basic-*Ppargc1a* reporter vector, and/or 0.6 μg of pCMV5/cMyc empty vector or pCMV5/cMyc-FCoR expression vectors. Synthetic Renilla luciferase reporter vector (phRL-SV40; Promega) (10 ng) was used as an internal control of transfection efficiency. After transfection, cells were cultured in DMEM containing 10% fetal calf serum and incubation was continued for 36 h. After that, cells were stimulated with forskolin (20 μM) for 6 h and the cells were harvested for luciferase assay.

To construct GAL4-Foxo1 expression vectors (PM-WT, -6KQ, and -6KR FoxO1), mouse Foxo1 cDNA was amplified by PCR using the pCMV5/cMyc-WT, -6KQ, or -6KR Foxo1 expression vectors as templates (Kitamura *et al*, 2005) and the following primers: 5′-GG *GGATCC* (*Bam*HI) GT ATG GCC GAG GCG CCC CAG GTG GTG-3′ (sense) and 5′-GG *GGATCC* (*Bam*HI) TTA GCC TGA CAC CCA GCT GTG TGT-3′ (antisense). After treatment with *Bam*HI, PCR products were subcloned into a *Bam*HI-treated pM vector (Clontech). To construct GAL4-Foxo3a, the Foxo3a cDNA fragment from *Eco*RI/*Hin*dII-treated PCMV5/cMyc/Foxo3a vector (Nakae *et al*, 2001) was ligated into an *Eco*RI/*Hin*dII-treated PM vector. To construct GAL4-FOXO4, human FOXO4 cDNA was amplified by PCR using PFN21AB7772 (Kazusa DNA Research Institute, Chiba, Japan) and the following primers: 5′-GG *GTCGAC* (*Sal*I) GCATGGATCCG GGGAATGAGAATTCA-3′ (sense) and 5′-GG *AAGCTT* (*Hin*dIII) TCAGGGATCTGGCTCAAAGTTGAA-3′ (antisense). After treatment with *Sal*I and *Hin*dIII, PCR products were subcloned into the *Sal*I/*Hin*dIII-treated pM vector. Plasmids were sequenced to confirm that they had the intended sequences. The 5XGAL4-luciferase reporter plasmid (pTAL-5XGAL4) was described previously (Katoh *et al*, 2006). For the 5XGAL4-luciferase assay, HEK293 cells were plated onto 12-well dishes. When the cells showed 70–80% confluence, transfections were carried out using 1.5 μg of pTAL-5XGAL4, 0.3 μg of several kinds of pM vector, and 0.6 μg of pCMV5/cMyc empty vector or pCMV5/cMyc-FCoR expression vectors. The synthetic Renilla luciferase reporter vector (phRL-SV40; Promega) (10 ng) was used as an internal control for transfection efficiency.

For luciferase assays using the J3-tk-Luc vector, HEK 293 cells were plated onto 12-well culture dishes. When the cells showed 70–80% confluence, transfections were carried out using 0.5 μg of the J3-tk-Luc reporter vector, 0.1 μg of pcDNA3-hPPARγ, 0.1 μg of pcDNA3-hRXRα, 0.1 μg of pFLAG-CNFoxo1 and/or 1.0 μg of pCMV5/cMyc empty vector or pCMV5/cMyc-FCoR expression vectors. The synthetic Renilla luciferase reporter vector (phRL-SV40; Promega) (10 ng) was used as an internal control for transfection efficiency. All vectors have been described previously (Vu-Dac *et al*, 1995; Tachibana *et al*, 2005). After transfection, cells were cultured in DMEM containing 10% fetal calf serum and incubation was continued for 36 h with 10 μM of rosiglitazone for 24 h.

Chip assay

3T3-F442A cells were seeded onto 15 cm-culture dishes and induced to differentiate into mature adipocytes as described previously (Nakae *et al*, 2003). On day 4 (clonal expansion) and day 6 (end of clonal expansion) after induction, cells were trypsinized and fixed with 1% formaldehyde for 1 h at 37°C. The DNA solution for Chip PCR was prepared according to the protocol in the Chip Assay Kit (Upstate). We performed immunoprecipitation with anti-FCoR serum, anti-FOXO1 (H128; Santa Cruz Biotechnology, Inc.), or an equal amount of normal rabbit IgG (Santa Cruz Biotechnology, Inc.). We subjected the samples to PCR using the following primers: for mouse *Cdkn1a*, 5′-aggaggaagactgggcatgtc-3′ and 5′-gagttggatcc ctagtaaggc-3′. For a Chip assay of *Ppargc1a* promoter, T37i cells infected with adenovirus encoding cMyc-FCoR were fixed with 1% formaldehyde for 1 h at 37°C. The DNA solution for the Chip assay was prepared as described previously (Nakae *et al*, 2006). We used an anti-cMyc mouse monoclonal antibody (9E10; Santa Cruz Biotechnology, Inc.) for immunoprecipitation of exogenous cMyc-FCoR. We subjected the samples to PCR using the following primers

for mouse *Ppargc1a*, S3: 5′-cctatgagatccacggaaag-3′ (sense) and 5′-cgctcctcatgtgatacatt-3′ (antisense), and S4: 5′-aatgtatcacatgagg agcg-3′ (sense) and 5′-ccagtcacatgacaaagcta-3′ (antisense).

Immunohistochemistry, immunofluorescence, and histological analysis

For histological analysis, we removed epididymal fat tissues from 20-week-old mice, fixed the specimens in 10% paraformaldehyde, and embedded them in paraffin. We mounted consecutive 10 μm sections on slides and stained them with haematoxylin and eosin. Measurement of WAT adipocyte size was performed using FLVFS-LS software (Flovel, Tokyo) by manually tracing at least 500 adipocytes for each genotype. Immunofluorescence using SV40-transformed hepatocytes or HEK293 cells was performed as described previously (Nakae *et al*, 2006). After transduction with adenoviruses encoding cMyc-FCoR and FLAG-3A FoxO1, cMyc-tagged FCoR was visualized in SV40-transformed hepatocytes with anti-cMyc monoclonal antibody and fluorescein isothiocyanate-conjugated anti-mouse IgG. FLAG-tagged CN FoxO1 was visualized with OctA-Probe (D-8) (sc-807, Santa Cruz Biotechnology, Inc.) and a Cy3-conjugated anti-rabbit IgG.

Statistics

We calculated descriptive statistics using ANOVA followed by Fisher's test (Statview; SAS Institute, Inc.). *P*-values of <0.05 were considered significant.

Supplementary data

Supplementary data are available at *The EMBO Journal* Online (http://www.embojournal.org).

Acknowledgements

We thank Dr Alan R Saltiel (University of Michigan, Ann Arbour, Michigan, USA) for providing the 3T3-L1 cDNA library, Dr Bruce M Spiegelman (Dana-Farber Cancer Institute, Boston, MA, USA) for providing promoter-enhancer fragment of the mouse *aP2* gene, Dr Tadahiro Kitamura (Laboratory of Metabolic Signal, Metabolic Signal Research Center, Gunma University, Japan) for providing the pCMV5-cMyc-6KQ and -6KQ FoxO1 expression vectors, and Dr Masao Doi and Dr Hitoshi Okamura (Department of System Biology, Kyoto University Graduate School of Pharmaceutical Science, Kyoto, Japan) for technical advice about the *in-vitro* acetylation assay. We also thank Dr Masato Kasuga (Research Institute, International Medical Centre of Japan, Tokyo, Japan) for helpful discussion. This work was supported by a grant for the 21st Century COE Program 'CenteR of Excellence for Signal Transduction Disease: Diabetes Mellitus as a Model' from the Ministry of Education, Culture, Sports, Science and Technology of Japan, Grants-in-Aid for Scientific Research for Priority Areas No. 18052013 from the Ministry of Education, Science, Sports, and Culture in Japan to JN; by a grant from the Takeda Science Foundation to JN; by a grant from the Astellas Foundation for Research on Metabolic Disorders to JN; by a grant from Novo Nordisk Insulin Research to JN; and by a grant from Nippon Boehringer Ingelheim Co. Ltd. to HI.

Author contributions: JN, HT, and ST designed the experiments. JN, YC, FH, YK, RS, TA, and HK carried out the experiments. TT and JS prepared vectors for the J3-tk-luciferase assay. JN and ST analysed all data. HI gave detailed comments of the paper. JN wrote the manuscript.

Conflict of interest

The authors declare that they have no conflict of interest.

References

Abel ED, Peroni O, Kim JK, Kim YB, Boss O, Hadro E, Minnemann T, Shulman GI, Kahn BB (2001) Adipose-selective targeting of the GLUT4 gene impairs insulin action in muscle and liver. *Nature* **409:** 729–733

Accili D, Arden KC (2004) FoxOs at the crossroads of cellular metabolism, differentiation, and transformation. *Cell* **117:** 421–426

Armoni M, Harel C, Karni S, Chen H, Bar-Yoseph F, Ver MR, Quon MJ, Karnieli E (2006) FOXO1 represses peroxisome proliferator-activated receptor-gamma1 and -gamma2 gene promoters in primary adipocytes. A novel paradigm to increase insulin sensitivity. *J Biol Chem* **281:** 19881–19891

Banks AS, Kim-Muller JY, Mastracci TL, Kofler NM, Qiang L, Haeusler RA, Jurczak MJ, Laznik D, Heinrich G, Samuel VT, Shulman GI, Papaioannou VE, Accili D (2011) Dissociation of the Glucose and Lipid Regulatory Functions of FoxO1 by Targeted Knockin of Acetylation-Defective Alleles in Mice. *Cell Metab* **14:** 587–597

Berdichevsky A, Viswanathan M, Horvitz HR, Guarente L (2006) C. elegans SIR-2.1 Interacts with 14-3-3 Proteins to Activate DAF-16 and Extend Life Span. *Cell* **125:** 1165–1177

Brunet A, Sweeney LB, Sturgill JF, Chua KF, Greer PL, Lin Y, Tran H, Ross SE, Mostoslavsky R, Cohen HY, Hu LS, Cheng HL, Jedrychowski MP, Gygi SP, Sinclair DA, Alt FW, Greenberg ME (2004) Stress-dependent regulation of FOXO transcription factors by the SIRT1 deacetylase. *Science* **303:** 2011–2015

Cannon B, Houstek J, Nedergaard J (1998) Brown adipose tissue. More than an effector of thermogenesis? *Ann NY Acad Sci* **856:** 171–187

Cao Y, Kamioka Y, Yokoi N, Kobayashi T, Hino O, Onodera M, Mochizuki N, Nakae J (2006) Interaction of FoxO1 and TSC2 induces insulin resistance through activation of the mammalian target of rapamycin/p70 S6K pathway. *J Biol Chem* **281:** 40242–40251

Daitoku H, Yamagata K, Matsuzaki H, Hatta M, Fukamizu A (2003) Regulation of PGC-1 promoter activity by protein kinase B and the forkhead transcription factor FKHR. *Diabetes* **52:** 642–649

Dowell P, Otto TC, Adi S, Lane MD (2003) Convergence of peroxisome proliferator-activated receptor gamma and Foxo1 signaling pathways. *J Biol Chem* **278:** 45485–45491

Fan W, Imamura T, Sonoda N, Sears DD, Patsouris D, Kim JJ, Olefsky JM (2009) FOXO1 transrepresses peroxisome proliferator-activated receptor gamma transactivation, coordinating an insulin-induced feed-forward response in adipocytes. *J Biol Chem* **284:** 12188–12197

Greer EL, Brunet A (2005) FOXO transcription factors at the interface between longevity and tumor suppression. *Oncogene* **24:** 7410–7425

He W, Barak Y, Hevener A, Olson P, Liao D, Le J, Nelson M, Ong E, Olefsky JM, Evans RM (2003) Adipose-specific peroxisome proliferator-activated receptor gamma knockout causes insulin resistance in fat and liver but not in muscle. *Proc Natl Acad Sci USA* **100:** 15712–15717

Imai T, Jiang M, Chambon P, Metzger D (2001) Impaired adipogenesis and lipolysis in the mouse upon selective ablation of the retinoid X receptor alpha mediated by a tamoxifen-inducible chimeric Cre recombinase (Cre-ERT2) in adipocytes. *Proc Natl Acad Sci USA* **98:** 224–228

Jing E, Gesta S, Kahn CR (2007) SIRT2 regulates adipocyte differentiation through FoxO1 acetylation/deacetylation. *Cell Metab* **6:** 105–114

Katoh Y, Takemori H, Lin XZ, Tamura M, Muraoka M, Satoh T, Tsuchiya Y, Min L, Doi J, Miyauchi A, Witters LA, Nakamura H, Okamoto M (2006) Silencing the constitutive active transcription factor CREB by the LKB1-SIK signaling cascade. *Febs J* **273:** 2730–2748

Kim JJ, Li P, Huntley J, Chang JP, Arden KC, Olefsky JM (2009) FoxO1 haploinsufficiency protects against high-fat diet-induced insulin resistance with enhanced peroxisome proliferator-activated receptor gamma activation in adipose tissue. *Diabetes* **58:** 1275–1282

Kitamura YI, Kitamura T, Kruse JP, Raum JC, Stein R, Gu W, Accili D (2005) FoxO1 protects against pancreatic beta cell failure through NeuroD and MafA induction. *Cell Metab* **2:** 153–163

Lefterova MI, Lazar MA (2009) New developments in adipogenesis. *Trends Endocrinol Metab* **20:** 107–114

Lochner A, Moolman JA (2006) The many faces of H89: a review. *Cardiovasc Drug Rev* **24:** 261–274

Matsumoto M, Han S, Kitamura T, Accili D (2006) Dual role of transcription factor FoxO1 in controlling hepatic insulin sensitivity and lipid metabolism. *J Clin Invest* **116:** 2464–2472

Mihaylova MM, Vasquez DS, Ravnskjaer K, Denechaud PD, Yu RT, Alvarez JG, Downes M, Evans RM, Montminy M, Shaw RJ (2011) Class IIa histone deacetylases are hormone-activated regulators of FOXO and mammalian glucose homeostasis. *Cell* **145:** 607–621

Nakae J, Barr V, Accili D (2000) Differential regulation of gene expression by insulin and IGF-1 receptors correlates with phosphorylation of a single amino acid residue in the forkhead transcription factor FKHR. *Embo J* **19:** 989–996

Nakae J, Cao Y, Daitoku H, Fukamizu A, Ogawa W, Yano Y, Hayashi Y (2006) The LXXLL motif of murine forkhead transcription factor FoxO1 mediates Sirt1-dependent transcriptional activity. *J Clin Invest* **116:** 2473–2483

Nakae J, Cao Y, Oki M, Orba Y, Sawa H, Kiyonari H, Iskandar K, Suga K, Lombes M, Hayashi Y (2008a) Forkhead transcription factor FoxO1 in adipose tissue regulates energy storage and expenditure. *Diabetes* **57:** 563–576

Nakae J, Kitamura T, Kitamura Y, Biggs 3rd WH, Arden KC, Accili D (2003) The forkhead transcription factor Foxo1 regulates adipocyte differentiation. *Dev Cell* **4:** 119–129

Nakae J, Kitamura T, Silver DL, Accili D (2001) The forkhead transcription factor Foxo1 (Fkhr) confers insulin sensitivity onto glucose-6-phosphatase expression. *J Clin Invest* **108:** 1359–1367

Nakae J, Oki M, Cao Y (2008b) The FoxO transcription factors and metabolic regulation. *FEBS Lett* **582:** 54–67

Nakae J, Park BC, Accili D (1999) Insulin stimulates phosphorylation of the forkhead transcription factor FKHR on serine 253 through a Wortmannin-sensitive pathway. *J Biol Chem* **274:** 15982–15985

Olefsky JM, Glass CK (2010) Macrophages, inflammation, and insulin resistance. *Annu Rev Physiol* **72:** 219–246

Printen JA, Brady MJ, Saltiel AR (1997) PTG, a protein phosphatase 1-binding protein with a role in glycogen metabolism. *Science* **275:** 1475–1478

Puigserver P, Rhee J, Donovan J, Walkey CJ, Yoon JC, Oriente F, Kitamura Y, Altomonte J, Dong H, Accili D, Spiegelman BM (2003) Insulin-regulated hepatic gluconeogenesis through FOXO1-PGC-1alpha interaction. *Nature* **423:** 550–555

Qiang L, Banks AS, Accili D (2010) Uncoupling of acetylation from phosphorylation regulates FoxO1 function independent of its subcellular localization. *J Biol Chem* **285:** 27396–27401

Tachibana K, Kobayashi Y, Tanaka T, Tagami M, Sugiyama A, Katayama T, Ueda C, Yamasaki D, Ishimoto K, Sumitomo M, Uchiyama Y, Kohro T, Sakai J, Hamakubo T, Kodama T, Doi T (2005) Gene expression profiling of potential peroxisome proliferator-activated receptor (PPAR) target genes in human hepatoblastoma cell lines inducibly expressing different PPAR isoforms. *Nucl Recept* **3:** 3

Takaishi H, Konishi H, Matsuzaki H, Ono Y, Shirai Y, Saito N, Kitamura T, Ogawa W, Kasuga M, Kikkawa U, Nishizuka Y (1999) Regulation of nuclear translocation of forkhead transcription factor AFX by protein kinase B. *Proc Natl Acad Sci USA* **96:** 11836–11841

Teleman AA, Chen YW, Cohen SM (2005) Drosophila melted modulates FOXO and TOR activity. *Dev Cell* **9:** 271–281

Vu-Dac N, Schoonjans K, Kosykh V, Dallongeville J, Fruchart JC, Staels B, Auwerx J (1995) Fibrates increase human apolipoprotein A-II expression through activation of the peroxisome proliferator-activated receptor. *J Clin Invest* **96:** 741–750

Wang B, Moya N, Niessen S, Hoover H, Mihaylova MM, Shaw RJ, Yates 3rd JR, Fischer WH, Thomas JB, Montminy M (2011) A hormone-dependent module regulating energy balance. *Cell* **145:** 596–606

Wolff S, Ma H, Burch D, Maciel GA, Hunter T, Dillin A (2006) SMK-1, an essential regulator of DAF-16-mediated longevity. *Cell* **124:** 1039–1053

Yagi T, Tokunaga T, Furuta Y, Nada S, Yoshida M, Tsukada T, Saga Y, Takeda N, Ikawa Y, Aizawa S (1993) A novel ES cell line, TT2, with high germline-differentiating potency. *Anal Biochem* **214:** 70–76

Yang Y, Hou H, Haller EM, Nicosia SV, Bai W (2005) Suppression of FOXO1 activity by FHL2 through SIRT1-mediated deacetylation. *EMBO J* **24:** 1021–1032

OPEN ACCESS Freely available online

PLOS ONE

Bile Acid Binding Resin Improves Metabolic Control through the Induction of Energy Expenditure

Mitsuhiro Watanabe[1,6]*, Kohkichi Morimoto[1], Sander M. Houten[2], Nao Kaneko-Iwasaki[1], Taichi Sugizaki[1], Yasushi Horai[1], Chikage Mataki[3], Hiroyuki Sato[4], Karin Murahashi[1], Eri Arita[1], Kristina Schoonjans[3], Tatsuya Suzuki[5], Hiroshi Itoh[1], Johan Auwerx[3]*

1 Department of Internal Medicine, School of Medicine, Keio University, Tokyo, Japan, **2** Laboratory Genetic Metabolic Diseases, Academic Medical Center, Amsterdam, The Netherlands, **3** Ecole Polytechnique Fédérale de Lausanne, Lausanne, Switzerland, **4** Department of Bioscience, Ehime University Graduate School of Medicine, Ehime, Japan, **5** Nippon Medical School, Tokyo, Japan, **6** Graduate School of Media and Governance, Keio University, Fujisawa-shi, Kanagawa, Japan

Abstract

Background: Besides well-established roles of bile acids (BA) in dietary lipid absorption and cholesterol homeostasis, it has recently become clear that BA is also a biological signaling molecule. We have shown that strategies aimed at activating TGR5 by increasing the BA pool size with BA administration may constitute a significant therapeutic advance to combat the metabolic syndrome and suggest that such strategies are worth testing in a clinical setting. Bile acid binding resin (BABR) is known not only to reduce serum cholesterol levels but also to improve glucose tolerance and insulin resistance in animal models and humans. However, the mechanisms by which BABR affects glucose homeostasis have not been established. We investigated how BABR affects glycemic control in diet-induced obesity models.

Methods and Findings: We evaluated the metabolic effect of BABR by administrating colestimide to animal models for the metabolic syndrome. Administration of BABR increased energy expenditure, translating into significant weight reduction and insulin sensitization. The metabolic effects of BABR coincide with activation of cholesterol and BA synthesis in liver and thermogenesis in brown adipose tissue. Interestingly, these effects of BABR occur despite normal food intake and triglyceride absorption. Administration of BABR and BA had similar effects on BA composition and thermogenesis, suggesting that they both are mediated *via* TGR5 activation.

Conclusion: Our data hence suggest that BABR could be useful for the management of the impaired glucose tolerance of the metabolic syndrome, since they not only lower cholesterol levels, but also reduce obesity and improve insulin resistance.

Citation: Watanabe M, Morimoto K, Houten SM, Kaneko-Iwasaki N, Sugizaki T, et al. (2012) Bile Acid Binding Resin Improves Metabolic Control through the Induction of Energy Expenditure. PLoS ONE 7(8): e38286. doi:10.1371/journal.pone.0038286

Editor: Massimo Federici, University of Tor Vergata, Italy

Received August 19, 2011; **Accepted** May 3, 2012; **Published** August 29, 2012

Funding: Funding was provided by grants of the Ecole Polytechnique Fédérale de Lausanne, the Swiss National Science Foundation, NIH, the Uehara Memorial Foundation, Takeda science foundation, the Sumitomo Foundation, Ono Medical Foundation, Astellas Foundation for Research on Metabolic Disorders, the Novartis Foundation (Japan) for Promotion of Science, the Japan Health Foundation, Kowa life science foundation and the Ministry of Education, Culture, Sports, Science and Technology of Japan for this study. The funders had no role in study design, data collection and analysis, decision to publish, or preparation of the manuscript.

Competing Interests: The authors have declared that no competing interests exist.

* E-mail: wmitsu@sc.itc.keio.ac.jp (MW); johan.auwerx@epfl.ch (JA)

Introduction

Bile acid (BA) is essential constituents of bile that facilitate dietary lipid absorption and cholesterol catabolism. BA also activates several signaling pathways, endowing them with an endocrine function. For instance, BA was shown to be natural ligands that activate the nuclear receptor farnesoid X receptor (FXR, NR1H4) [1–3], which controls both the synthesis and enterohepatic circulation of BA [4–5]. FXR induces the expression of the short heterodimer partner (SHP, NR0B2), an atypical nuclear receptor that acts as a corepressor. The FXR-mediated SHP induction contributes to the negative feedback regulation of BA biosynthesis, through inhibition of liver X receptor α and β (LXRα, NR1H3 and LXRβ, NR1H2) and liver receptor homolog-1 (LRH-1, NR5A2), both required for the transcription of the rate-limiting enzyme in the neutral BA biosynthesis pathway, cholesterol 7α-hydroxylase (CYP7A1) [6–11]. The FXR-mediated induction of FGF15/19 (FGF19 in human and its ortholog FGF15 in mouse) in intestinal epithelial cells also participates in the feedback repression of BA synthesis, via FGFR4 on hepatocytes [12–14]. Using a similar mechanism, the FXR-mediated SHP induction attenuates the capacity of LXR and LRH-1 to induce the expression of sterol regulatory element-binding protein (SREBP)-1c, the master regulator of lipogenesis, explaining the inhibition of hepatic fatty acid and triglyceride biosynthesis and VLDL production by BA administration [15]. Recently, it was reported that FXR deficiency improves glucose homeostasis in a mouse model for the metabolic syndrome [16]. In addition, we established that a synthetic FXR agonist (GW4064), deteriorates metabolic control in a diet-induced obesity mouse model [17]. These results suggest that the BA-specific nuclear

receptor FXR is involved in the pathogenesis of the metabolic syndrome.

BA may also signal in peripheral tissues through another pathway involving the binding and activation of TGR5, a G protein-coupled receptor (GPCR), leading to the induction of intracellular cyclic adenosine monophosphate (cAMP) levels [18–19]. The subsequent activation of type 2 iodothyronine deiodinase (D2), the enzyme which converts inactive thyroxine into active 3,5,3′-triiodothyronine [20] and hence determines thyroid hormone receptor saturation in cells, and of peroxisome proliferator-activated receptor (PPAR) γ coactivator-1α (PGC-1α), the master regulator of mitochondrial biogenesis [21], then stimulates energy expenditure in brown adipose tissue (BAT) (in rodents) and skeletal muscle (in humans) [22].Activation of this pathway explains how administration of BA to mouse models of obesity and diabetes induces weight loss and insulin sensitization. In addition, we reported that in mice, a synthetic FXR agonist (GW4064) reduced the BA pool and altered BA composition impairing peripheral energy metabolism possibly *via* TGR5 [17]. Furthermore, TGR5 activation enhances GLP-1 secretion from the enteroendocrine L-cell stimulating pancreatic insulin secretion [23]. Thus in addition to FXR, the BA-specific GPCR TGR5, is an attractive therapeutic target for treating metabolic syndrome.

These observations have built a strong case that BA has effects beyond the strict control of BA homeostasis and function as general metabolic integrators [24]. Bile acid binding resins (BABR), such as cholestyramine, is effective drugs for the treatment of coronary heart disease by lowering LDL-cholesterol as primary prevention, and for the treatment of cholestatic liver disease. BABR absorbs BA in the intestine thereby preventing their uptake in the ileum and interrupting their enterohepatic circulation. The resulting decrease of negative feedback signals will induce the expression of *Cyp7a1*. The subsequent decrease in intrahepatic cholesterol levels will on its turn activate SREBP-2, which induces the expression of the low density lipoprotein (LDL) receptor, to enhance cholesterol uptake, and of enzymes that synthesize cholesterol de novo, such as 3-hydroxy-3-methylglutaryl (HMG) CoA reductase. BABR was also reported to improve glycemic control in a type 2 diabetes mouse model [25], but the mechanism has not been established. We characterize here in detail the molecular and functional impact of a second generation BABR, colestimide [26], on metabolic homeostasis in animal models for the metabolic syndrome. Interestingly, colestimide not only reduces cholesterol levels but also decreases body weight and improves glucose tolerance, qualifying BABR as ideal agents to treat the metabolic syndrome. We suggest that a part of the anti-metabolic syndrome effect of BABR will be exerted by an alteration of the peripheral BA composition followed by TGR5 activation.

Materials and Methods

Materials

Cholic acid (CA) and cholestyramine were obtained from Sigma (St. Quentin Fallavier, France). Colestimide was a generous gift of Mitsubishi Pharmaceuticals.

Animal studies

All procedures undertaken in the present study conformed to the principles outlined in the *Guide for the Care and Use of Laboratory Animals* published by the USA National Institutes of Health (NIH Publication No. 85-23, revised 1996) and were approved by the Institutional Animal Care and Use Committee of Keio University School of Medicine (permission No. 08062-(2)). Male C57BL/6J mice, 6–7 weeks of age, were obtained from Charles River Laboratories France (l'Arbresle, France) and CLEA Japan Inc. (Tokyo, Japan), respectively. All mice were maintained in a temperature-controlled (23°C) facility with a 12 hours light/dark cycle and were given free access to food and water. The high-fat diet was obtained from Research diets (New Jersey, USA). The high-fat diet (D12492) contained 20 kcal% protein, 20 kcal% carbohydrate and 60 kcal% fat. For treatment with BA or BABR, mice were fed diets mixed with CA (0.5% w/w) or colestimide (2% w/w). Based on a daily food intake of 5 g, this resulted in a daily dose of colestimide 100 mg. The mice were fasted 4 hours before harvesting blood for subsequent blood measurements, and tissues for RNA isolation, lipid measurements and histology. Food intake was measured from the accumulated weight of the food for 1 week, with 5 mice in each group. Oxygen consumption was measured using the Oxymax apparatus (Columbus Instruments, Columbus, OH) [27].

Morphological studies

Pieces of mouse tissues were fixed in Bouin's solution, dehydrated in ethanol, embedded in paraffin, and cut at a thickness of 5 μm. Sections were deparaffinized, rehydrated, and stained with haematoxylin and eosin.

mRNA expression analysis by Q-RT-PCR

Expression levels were analyzed in cDNA synthesized from total mRNA using real-time PCR as described [22]. The sequences of the primer sets used are displayed in table 1.

Clinical biochemistry and evaluation of glucose and lipid homeostasis

An oral glucose tolerance test (OGTT) was performed in animals that were fasted overnight. Glucose was administered by gavage at a dose of 2 g/kg. An intra peritoneal insulin tolerance test (IPITT) was done in 4 h fasted animals. Insulin was injected at a dose of 0.75 U/kg. Glucose quantification was done with the Maxi Kit Glucometer 4 (Bayer Diagnostic, Puteaux, France) or Glucose RTU (bioMérieux Inc., Marcy l'Etoile, France). Plasma insulin concentrations were measured using ELISA for mouse (Cristal Chem Inc., Downers Grove, IL). HOMA-R was calculated by this formula: (fasting serum insulin concentration [μU/ml])*(fasting serum glucose concentration [mg/dl])/405. Free fatty acids, triglycerides, and total cholesterol were determined by enzymatic assays (Roche, Mannheim, Germany). LDL cholesterol was measured with plasma clinical chemistry analysis using AU-400 automated laboratory workstation and commercial reagents (Olympus France SA, Rungis, France) [28]. BA in enterohepatic organs were determined as described [29]. Lipid absorption was calculated as follows; (food lipid content – fecal lipid content)/food lipid content (×100(%)), with the food and feces consumed by/accumulated from 5 mice for 48 hours. To calculate the lipid absorption, TG was extracted from the accumulated feces by the classical Folch method [30] and measured as previously described [15].

Statistical analysis

Values were reported as mean +/− standard error (SEM). Statistical differences were determined using ANOVA (Statsview software, Abacus concepts, Inc., Berkeley, CA). Statistical significance is displayed as * ($P<0.05$) or ** ($P<0.01$) versus F.

Table 1. Primer sequences of genes used for quantification of mRNAs by real-time PCR.

Gene	Forward Primer (5′→3′)	Reverse Primer (5′→3′)
18s	GATGGGAAGTACAGCCAGGT	TTTCTTCAGCCTCTCCAGGT
Cyp7A1	TACAGAGTGCTGGCCAAGAG	TTCAAGGATGCACTGGAGAG
SHP	CAAGGAGTATGCGTACCTGAAG	GGCTCCAAGACTTCACACAGT
FXR	CAAAATGACTCAGGAGGAGTACG	GCCTCTCTGTCCTTGATGTATTG
PGC-1a	AAGGGCCAAACAGAGAGAGA	GCGTTGTGTCAGGTCTGATT
PEPCK	GGGAACTCACTACTCGGGAA	GCCAGGTATTTCTTCTTGCC
G6Pase	CCGGATCTACCTTGCTGCTCACTTT	TAGCAGGTAGAATCCAAGCGCGAAAC
SREBP-2	AAGTGACCGAGAGTCCCTTG	ACGTTGAGACTGCTCCACAG
HMGCR	TCGAAGGACGAGGAAAGACT	CGTCAACCATAGCTTCCGTA
LDLR	AGGCTGTGGGCTCCATAGG	TGCGGTCCAGGGTCATCT
PPARa	GGTGAGGAGAGCTCTGGAAG	GAAGCTGGAGAGAGGGTGTC
ACC	ACCCACTCCACTGTTTGTGA	CCTTGGAATTCAGGAGAGGA
SCD1	CTCCTGCTGATGTGCTTCAT	AAGGTGCTAACGAACAGGCT
D2	TTCTGAGCCGCTCCAAGT	GGAGCATCTTCACCCAGTTT
UCP-1	GGCCCTTGTAAACAACAAAATAC	GGCAACAAGAGCTGACAGTAAAT
FGF15	GGCAAGATATACGGGCTGAT	GATGGTGCTTCATGGATCTG
mCPT-1	GCACTGCAGCTCGCACATTACAA	CTCAGACAGTACCTCCTTCAGGAAA
Cyp8B1	GGAAGCCAAGAAGTCGTTCA	GACGCAGACTCTCCTCCATC
Cyp27A1	TCTGGCTACCTGCACTTCCT	CTGGATCTCTGGGCTCTTTG

doi:10.1371/journal.pone.0038286.t001

Results

BABR prevents the onset of diet-induced obesity

To evaluate the metabolic effects of a BABR in models of diet-induced obesity (DIO), we fed C57BL/6J mice normal chow, HF diet, or HF diet supplemented with either colestimide (2% w/w) or cholic acid (CA, 0.5% w/w) for 96 days. HF fed animals gained more weight than chow-fed animals. The animals fed with CA supplemented HF diet gained weight at a rate comparable to chow-fed mice. Colestimide had an even more pronounced effect in curbing weight gain. Since food intake and lipid absorption were not affected by CA and colestimide, these effects on body weight are probably mediated by increased energy expenditure (Fig. 1A). At necropsy, the weight of liver, epididymal white adipose tissue (epWAT) and BAT of HF fed animals was all significantly increased (Fig. 1B). The BAT was paler, indicative of increased fat accumulation, and there was an expansion of WAT surrounding the BAT (not shown). Both colestimide and CA completely prevented HF-induced changes in liver and adipose mass and morphology. High fat diet-induced significantly increased serum total cholesterol (T-C), LDL-cholesterol (LDL-C), fasting glucose and insulin levels. Colestimide ameliorated serum triglyceride (TG), T-C, LDL-C, fasting glucose and insulin levels significantly. CA administration exerted significant reduction of fasting glucose and insulin levels, but induced serum LDL-C level as expected (Fig. 1C). During OGTT, both colestimide and CA significantly reduced blood glucose concentrations to normalize the glucose tolerance of the mice with diet-induced obesity. Insulin sensitivity of the mice was also improved by colestimide and CA, shown in the result of IPITT (Fig. 1D). In KK-A^y mice, both colestimide and cholestiramine improved metabolic status (Text S1) without suppressing their food intake (Fig. S1A). The BABR significantly reduced epWAT weight gain, and also significantly improved serum metabolic index including TG, FFA, fasting glucose, insulin levels, and HOMA-R. Colestimide administration significantly improved liver weight gain and serum T-C level, either (Fig. S1B–D). The BABR-received KK-A^y mice exhibited significantly lower blood glucose during the OGTT (Fig. S1E). In the IPITT, the BABR reduced blood glucose level, but the improvement rate described in iAUC was not affected by the BABR administration (Fig. S1E). These data show that BABR improves metabolic control in mouse models for the metabolic syndrome.

BABR increases energy expenditure

The significant weight loss, in the wake of an unaltered food intake, suggested that BABR could stimulate energy expenditure and as such improve metabolic homeostasis. We hence analyzed the morphology of key metabolic tissues and performed indirect calorimetry in the C57BL/6J mice used in the HF study (see Fig. 1). This furthermore enabled us to compare the effect of the BABR with those of BA, which we characterized previously in this model [15] [22]. Liver sections of HF fed animals showed more unstained inclusions, indicative of steatosis, which were absent when the HF diet was supplemented with colestimide or CA (not shown and [15]). The HF diet induced significant adipocyte hypertrophy in both epWAT, characterized by a larger adipocyte volume (Fig. 2A), and BAT, typified by larger lipid vacuoles within the cells. This adipocyte hypertrophy was not observed when the HF diet was supplemented with either colestimide or CA. Electron microscopic analysis of BAT also showed more lipid vacuoles in HF fed animals when compared with chow fed animals or animals receiving HF diet combined with colestimide or CA (Fig. 2A,B&C). Compared with the HF diet, colestimide and CA supplementation increased the number of lamellar cristae in the mitochondria (Fig. 2C). Indirect calorimetry, showed a higher CO_2 production and O_2 consumption in animals fed a HF diet with either colestimide or CA when compared to animals on a HF or a

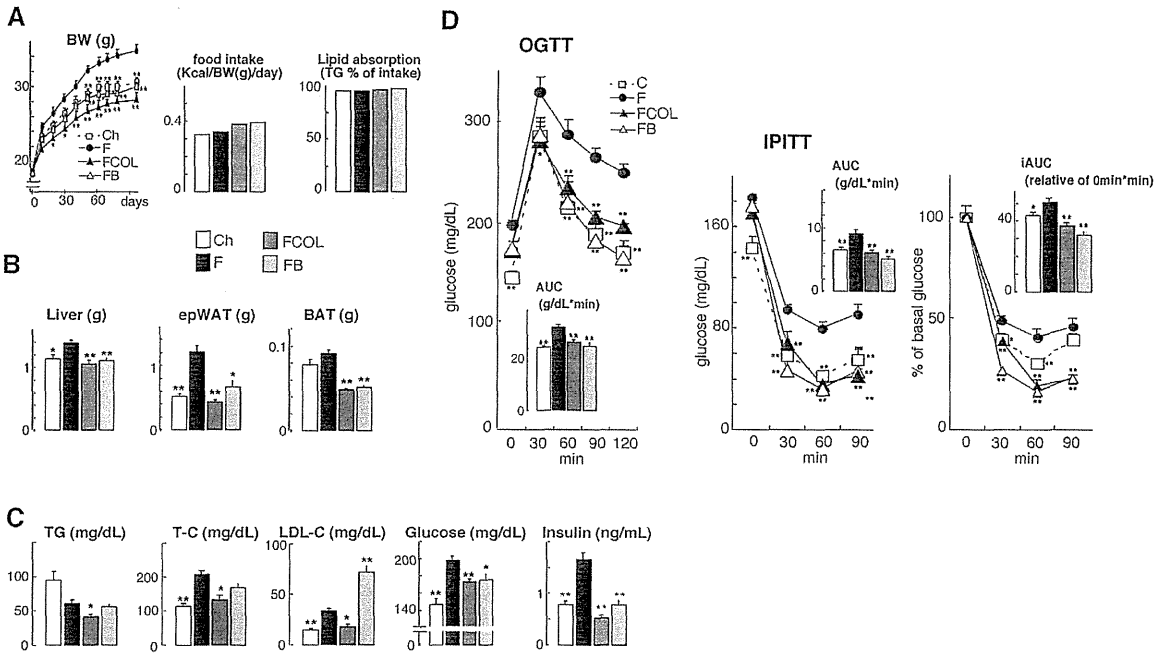

Figure 1. BA and BABR improve metabolic control in DIO C57BL/6J mice model. (A) Body weight, food intake and TG absorption (B) Liver, epididymal WAT (epWAT), and BAT weight change of C57BL/6J mice during 96 days on different diets. Ch stands for chow, F denotes HF diet, FCOL denotes HF diet+2.0% w/w colestimide and FB denotes HF diet+0.5% w/w CA. (C) Serum levels of TG, T-C, LDL-C, glucose and insulin in C57BL/6J mice on the indicated treatments. (D) Glucose levels during OGTT and IPITT in the different treatment groups (AUC is depicted in the inset). The OGTT were performed after an overnight fast after 9 weeks of administration. Glucose was administered by gavage at a dose of 2 g/kg. The IPITT were performed after 4 h fast after 10 weeks of administration. Insulin was injected at a dose of 0.75 U/kg. Data are expressed as the mean +/− SEM (n = 5–6). * ($P<0.05$) or ** ($P<0.01$) versus F.
doi:10.1371/journal.pone.0038286.g001

normal diet (Fig. 2D). We conclude from these experiments that feeding of colestimide or CA changes fat and energy metabolism most likely due to an effect on basal metabolic rate.

Molecular mechanism of BABR action

To identify the molecular drivers of the effects of BABR, we performed analysis of gene expression using Q-RT-PCR in liver, BAT, muscle and ileum of the C57BL/6J HF study (Fig. 1). Hepatic gene expression reflected the interruption of the enterohepatic cycle of BA by BABR and its consequences on BA production and cholesterol homeostasis. These changes were typified by the significant induction of *Cyp7a1* expression, subusequent to the reduction in *Shp*. *Cyp8b1* expression was significantly suppressed by CA administration, but was not affected by BABR administration. Gene expression of *Cyp27a1*, another rate-limiting enzyme participating in the alternative acidic BA synthesis pathway, was not affected by CA or BABR administration. The cholesterol depletion caused by colestimide stimulated BA production by CYP7A1, and then induced significantly increased expression levels of *Srebp-2* and its target genes including HMG-CoA reductase and LDL receptor. Genes involved in gluconeogenesis, such as phosphoenolpyruvate carboxykinase (*Pepck*) and glucose-6-phophatase (*G6Pase*) were affected. *Pepck* gene expression was significantly induced, and *G6Pase* gene expression was also stimulated as a consequence of the significant rise in the *Pgc-1a* expression, which stimulates gluconeogenesis. In contrast to colestimide, and as previously reported, the FXR agonist CA significantly induced *Shp* mRNA levels, which attenuates the expression of *Cyp7a1* and of the genes involved in cholesterol homeostasis. Genes involved in fatty acid oxidation (*Pparα*) and lipogenesis (acetyl-CoA carboxylase 1 (*Acc1*) and stearoyl-CoA desaturase-1 (*Scd1*)) were not changed in response to colestimide and CA (Fig. 3A).

In BAT, the expression of *Pgc-1α* and *D2* were both induced by colestimide and CA. As a consequence the expression of uncoupling protein-1 (*Ucp-1*) was also increased after both BABR and BA administration (Fig. 3B). Colestimide and CA treatment did not lead to significant differences in the expression of the genes involved in energy homeostasis in muscle (Fig. 3C). In ileum, the expression of *Fgf15*, which is one of the target genes of FXR, was significantly decreased by colestimide and increased by CA (Fig. 3D). In combination, the gene expression studies confirm that BAT and liver are the primary target organs that contribute to the beneficial effects of BABR on energy, lipid and glucose homeostasis. Remarkably, the effect on energy homeostasis induced by BABR was very similar to those observed after administration of CA (Figs. 1, 2, 3, Fig. S1 and [22]), despite the fact that BABR and BA has opposite actions on hepatic gene expression. Precisely, BABR administration induces *Cyp7a1* expression, while BA supplementation reduces expression of this gene, which is secondary to the changes in the BA pool size and serum BA levels. CA increased the BA pool and serum BA levels, but unexpectedly colestimide induced only a minor and non significant decrease in these parameters (Table 2). More striking, the changes in the composition of the BA pool and serum BA was similar after BABR or CA administration [22]. Both treatments